Self-Healing Hydrogels Formed via Hydrophobic Interactions

Oguz Okay

Contents

Abstract Hydrogels are physically or chemically cross-linked polymers with the ability to absorb large amounts of water without dissolving. Elasticity, smartness, and high water sorption capacity make hydrogels extraordinary materials. Although synthetic hydrogels resemble biological tissue, they generally exhibit poor mechanical performance, which limits their use in stress-bearing applications. Hence, synthetic hydrogels that combine good mechanical properties with stimuli-responsiveness and self-healing ability are required for the development of several new technologies. To create such high-toughness hydrogels with self-healing abilities, hydrophobic modification of hydrophilic polymer chains has attracted great interest in recent years. Incorporation of a small amount of hydrophobic units with long alkyl side chains into hydrophilic polymers creates an energy dissipation mechanism. This mechanism appears as a result of the hydrophobic associations, i.e., reversible cross-links within the polymer network. Hydrogels formed via hydrophobic interactions in micellar solutions exhibit unique properties such as a high stretchability (up to 5,000 %), high mechanical strength (up to 1.7 MPa tensile stress), and complete autonomous self-healing ability. Mixed

O. Okay (✉)
Department of Chemistry, Istanbul Technical University, 34469 Maslak, Istanbul, Turkey
e-mail: okayo@itu.edu.tr

S. Seiffert (ed.), *Supramolecular Polymer Networks and Gels*, Advances in Polymer Science 268, DOI 10.1007/978-3-319-15404-6_3

micelles acting as physical cross-links in these hydrogels are formed by dynamic hydrophobic association between the hydrophobic domains of the polymer chains and grown surfactant micelles. This chapter describes some conditions for formation of hydrophobically modified hydrogels with extraordinary mechanical properties and self-healing abilities. Special emphasis is placed on the role of surfactant micelles for the dynamic and mechanical properties of these hydrophobically modified hydrogels.

Keywords Dynamics • Hydrogels • Hydrophobic associations • Mechanical properties • Self-healing

Abbreviations

AAc	Acrylic acid
AAm	Acrylamide
AIBN	2,2′-Azobis(isobutyronitrile)
APS	Ammonium persulfate
C16M	*N*-Hexadecyl methacrylate
C17.3M	Stearyl methacrylate
C18A	*N*-Octadecyl acrylate
C18M	*N*-Octadecyl methacrylate
C22A	Dococyl acrylate
C_0	Initial monomer concentration
CTAB	Cetyltrimethylammonium bromide
D	Cooperative diffusion coefficient
D_A	Apparent diffusion coefficient
DLS	Dynamic light scattering
DMA	*N*,*N*-Dimethylacrylamide
DMSO	Dimethyl sulfoxide
E	Tensile modulus
f_{HM}	Mole fraction of hydrophobic monomer in the comonomer feed
f_ν	Fraction of associations broken during the loading
G	Shear modulus
$G(t)$	Relaxation modulus
G'	Elastic modulus
G''	Viscous modulus
G_R	Rouse modulus
HM	Hydrophobically modified
$<I>_E$	Ensemble-averaged scattering intensity
$I_C(q)$	Scattered intensity as a result of the frozen structure
$<I(q)>_T$	Time-averaged scattering intensity
$<I_F(q)>_T$	Scattered intensity as a result of the liquid-like concentration fluctuations

ICF	Time average intensity correlation function
m_{rel}	Relative gel mass
$m_{rel,eq}$	Equilibrium swelling ratio
n	Refractive index
N	Polymer chain length
N_{Agg}	Aggregation number of the surfactant
N_H	Number of hydrophobes per hydrophobic block
PAAc	Poly(acrylic acid)
PAAm	Polyacrylamide
PDMA	Poly(*N*,*N*-dimethylacrylamide)
q	Scattering vector
SDS	Sodium dodecylsulfate
SMS	Sodium metabisulfite
S_n	Number of hydrophobic blocks per chain
$\tan \delta$	Loss factor (equal to G''/G')
TEMED	*N*,*N*,*N*′,*N*′-Tetramethylethylenediamine
U_{hys}	Hysteresis energy
U_{xl}	Average dissociation energy of a single association
β	Molar ratio of CTAB to the AAc units in the polymer
β_0	CTAB/AAc molar ratio in the gelation solution
γ_c	Critical shear rate for shear thickening
Γ_{fast}	Relaxation rate of the fast mode
γ_0	Strain amplitude
Γ_{slow}	Relaxation rate of the slow mode
η	Viscosity
η_{sp}	Specific viscosity
θ	Scattering angle
λ	Deformation ratio
$\lambda_{biax,max}$	Maximum biaxial extension ratio
λ_f	Stretch at failure
λ_{max}	Maximum strain
ν_e	Effective cross-linking density
ξ	Dynamic correlation length
ξ_H	Hydrodynamic correlation length
σ_f	Fracture stress
σ_{nom}	Nominal stress
σ_{true}	True stress
τ	Decay time
τ_1	Lifetime of associations
τ_c	Characteristic time (equal to ${\gamma_c}^{-1}$)
τ_R	Characteristic relaxation time (equal to ${\omega_c}^{-1}$)
ω	Angular frequency
ω_c	Cross-over frequency at which G' and G'' are equal in oscillatory shear rheology

1 Introduction

Hydrogels are similar to biological tissue in that they consist of three-dimensional networks of macromolecules and water as the main component. Elasticity, smartness, and high water sorption capacity make hydrogels extraordinary materials [1]. However, synthetic hydrogels prepared by classical chemical methods are normally brittle, which limits their use in stress-bearing applications. Therefore, design of hydrogels with good mechanical properties is crucial. Synthetic hydrogels that combine high toughness with stimuli-responsiveness and self-healing ability are promising for the development of several new technologies.

The poor mechanical performance of chemical hydrogels mainly arises from their low resistance to crack propagation because of the lack of an efficient energy dissipation mechanism in the gel network [2, 3]. As demonstrated by the cartoon in Fig. 1a, the energy accumulated close to a crack tip cannot be dissipated in chemical hydrogels, leading to fracture of the material [4]. Hence, to obtain high-toughness hydrogels, the overall viscoelastic dissipation along the hydrogel sample should be increased by introducing dissipative mechanisms at a molecular level. To improve the mechanical properties of conventional hydrogels, many studies have been conducted in recent years [5–11]. Moreover, inspired by natural healing processes, different reversible molecular interactions have been used to generate hydrogels with the ability to self-heal, autonomously or with the help of an external stimulus [12–30].

To create high-toughness hydrogels with self-healing abilities, hydrophobic modification of hydrophilic polymer chains has attracted great interest [4, 8, 31–42]. Incorporation of a small amount of hydrophobic units with long alkyl side chains in a hydrophilic polymer backbone dramatically increases the viscous modulus, G'', of aqueous polymer solutions, reflecting creation of energy dissipation mechanisms as a result of the formation of hydrophobic associations (i.e., temporary junction zones inside the gel network). The driving force for the formation of these associations is the interaction between the hydrophobic groups, which arises in order to minimize their exposure to water. The activation energy for the disengagement of hydrophobes from these associations is in the order of the thermal energy kT [43–47], so that the free and bonded hydrophobes in such physical gels are in a dynamic equilibrium. As illustrated in Fig. 1b, the crack energy along the hydrogel is dissipated by reversible disengagement of the hydrophobes from their hydrophobic associations, so that growth of a crack to a macroscopic level can be prevented. Over the past few years, intensive studies have been conducted with the aim of developing high-toughness self-healing physical hydrogels via hydrophobic interactions [32–42]. Figure 2a–c schematically depicts the strategy used for the preparation of such hydrogels. Mixed micelles acting as physical cross-links in the hydrogels are formed by dynamic hydrophobic association of the hydrophobic domains of hydrophilic polymer chains and grown surfactant micelles. Hydrogels formed via such hydrophobic interactions in micellar solutions exhibit unique

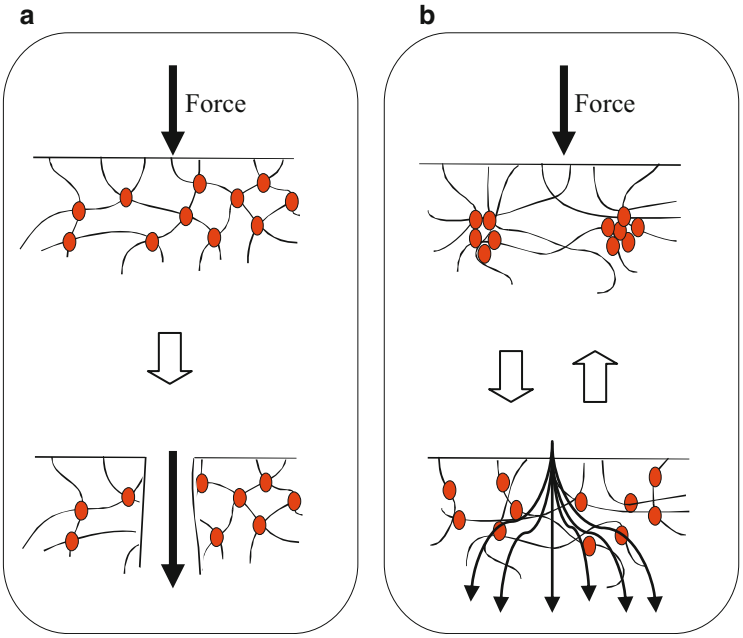

Fig. 1 (**a**) Formation of a crack in a chemical hydrogel with no viscous dissipation. (**b**) Energy dissipation in a hydrogel formed via hydrophobic interactions. From [4] with permission from Elsevier

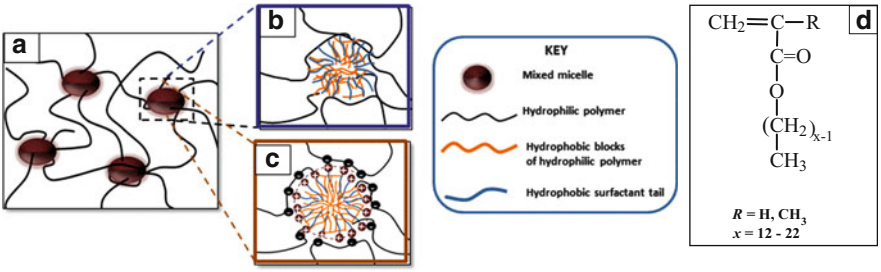

Fig. 2 (**a–c**) Physical polymer-network cross-linking provided by mixed micelles in hydrogels formed via hydrophobic interactions in surfactant solutions. Mixed micelles are formed by aggregation of hydrophobic blocks of per-se hydrophilic polymers and surfactant alkyl tails. (**b**) Nonionic polymer and ionic surfactant gel system at the state of preparation. For clarity, charges are not shown. (**c**) Ionic polymer and oppositely charged surfactant gel system after extraction of free micelles. (**d**) Structure of the hydrophobic monomers used in the micellar polymerization

properties such as a high stretchability (up to 5,000 %), high mechanical strength (up to 1.7 MPa tensile stress), and complete autonomous self-healing.

This chapter discusses formation conditions as well as rheological and mechanical properties of hydrogels formed via hydrophobic associations in micellar solutions; it also discusses why the dynamic and mechanical properties of such

hydrogels significantly differ from conventional gels formed by chemical cross-linkers. The extraordinary mechanical properties, including self-healing, are also discussed.

2 Preparation of Hydrophobically Modified Hydrogels

Hydrogels formed via hydrophobic interactions are mainly prepared by copolymerization of a hydrophilic monomer with a small amount (1–5 mol%) of a hydrophobic comonomer, most typically by a free-radical mechanism. Acrylamide (AAm), *N*,*N*-dimethylacrylamide (DMA), or acrylic acid (AAc) are mainly used as the hydrophilic monomer in the precursor-polymer preparation. Several hydrocarbon hydrophobes, including *N*-alkyl-, *N*,*N*-dialkyl-acrylamides or -(meth)acrylates of various alkyl chain length, and fluorocarbon hydrophobes such as 2-(*N*-ethylperfluorooctane sulfonamido)ethyl acrylate have been used for the preparation of physical gels from these precursor polymers [4, 31, 48, 49]. To create strong hydrophobic interactions between the hydrophilic polymer chains, hydrophobic acrylates or methacrylates with an alkyl chain length of between 12 and 22 carbon atoms are generally used (Fig. 2d). In this chapter, the hydrophobes are named C*x*R, where C represents carbon, *x* is the number of carbons in side alkyl chain, and R refers to A or M for acrylates and methacrylates, respectively. For instance, C18M and C16M stand for *n*-octadecyl methacrylate and *n*-hexadecyl methacrylate, respectively. Because stearyl methacrylate (C17.3M) consists of 65 % C18M and 35 % C16M, its average chain length, 17.3, is used in its short name.

Because hydrophilic monomers are soluble in water, whereas hydrophobes are insoluble, a common solvent or solvent mixture needs to be used for their copolymerization. Ethanol is a common solvent able to dissolve both AAc and C18A, so that their copolymerization can be conducted in this medium using free-radical initiators such as 2,2′-azobis(isobutyronitrile) (AIBN) [50]. Similarly, free-radical copolymerization of DMA with 5–22 mol% of 2-(*N*-ethylperfluorooctane sulfonamido)ethyl acrylate can be conducted in dioxane [48]. Another approach for the creation of hydrophobically modified hydrophilic polymers is polymer-analogous hydrophobic modification of preformed hydrophilic chains. For instance, hydrophobically modified poly(acrylic acid) (PAAc) can be prepared by grafting dodecyl amine onto the carboxylic acids of a PAAc backbone in the presence of dicyclohexylcarbodimide [8]. In contrast to this complicated procedure, a simple way for the synthesis of hydrophobically modified polymers is the micellar polymerization technique [51–58]. A particular advantage of this approach is the blocky structure of the resulting polymers, significantly enhancing their associative properties. In this technique, a hydrophobic monomer is first solubilized within micelles, and then it is copolymerized with a hydrophilic monomer in aqueous solution by a free-radical mechanism. Surfactants such as sodium dodecylsulfate (SDS) or cetyltrimethylammonium bromide (CTAB) serve for the solubilization of the hydrophobes in aqueous solution. Usually, redox-initiators such as ammonium

persulfate (APS) along with *N*,*N*,*N*′,*N*′-tetramethylethylenediamine (TEMED) or APS along with sodium metabisulfite (SMS) are used to initiate the reactions at ambient temperatures. Because the Krafft point for CTAB in water is around 20–25 °C [59], the reactions in CTAB solutions are carried out at elevated temperatures, 35–50 °C. As a result of the high concentration of hydrophobic monomer within the micelles, the hydrophobes are randomly distributed as blocks along the hydrophilic polymer chains. The number of hydrophobic monomeric units per hydrophobic block (N_H) and the number of blocks per chain (S_n) can be estimated from the molar concentration ratio of hydrophobic monomer (HM) to the surfactant (S) by:

$$N_H = \frac{[HM]N_{Agg}}{[S] - CMC} \tag{1a}$$

$$S_n = \frac{f_{HM}N}{N_H} \tag{1b}$$

where N_{Agg} is the aggregation number of the surfactant, CMC is its critical micelle concentration, f_{HM} is the mole fraction of HM in the comonomer feed, and N is the chain length of polymer [53]. Because incorporation of a small amount of hydrophobic groups in a hydrophilic polymer backbone results in polymers with extraordinary rheological properties in aqueous solutions, many studies have been carried out during the past two decades on the synthesis and solution properties of hydrophobically modified hydrophilic polymers [54, 55]. Candau and coworkers investigated the preparation and rheological behavior of polyacrylamides (PAAms) modified with various amounts of *N*-alkyl- or *N*,*N*-dialkylacrylamides of various alkyl-chain lengths [51–54, 56–58]. The zero-shear viscosity of semidilute solutions of hydrophobically modified polymers significantly increases as the number of hydrophobes per block (N_H) or the number of blocks per chain (S_n) is increased [52, 56, 57]. Hydrophobically modified PAAms are of great interest due to their possible application areas, including oil recovery and paints.

Physical hydrogels derived from hydrophobically modified hydrophilic polymers drew much less interest in the past, but they have recently attracted intense attention because of their extraordinary properties [4, 8, 31–42]. To produce mechanically strong hydrogels via micellar copolymerization, blocks of hydrophobes with long alkyl side chains such as *n*-octadecyl acrylate (C18A) or dococyl acrylate (C22A) should be incorporated into the hydrophilic backbone [32, 34]. However, although hydrophobes with an alkyl-chain length of up to 12 carbon atoms can easily be copolymerized with hydrophilic monomers, larger hydrophobes cannot be copolymerized in micellar solutions. This is a result of the low solubility of large hydrophobes in water (e.g., 10^{-9} mL mL^{-1} for C18M [60]), which limits their transport into the micelles [61, 62]. To solve this challenge, salts such as NaCl or NaBr were added to the micellar solution [32]; this weakened electrostatic interactions and caused the micelles to grow [63–67], which, in turn, provided solubilization of large amounts of hydrophobes in the micellar solution. Figure 3a, b demonstrates the NaCl-induced solubilization of C18A in an aqueous 22 % (w/v)

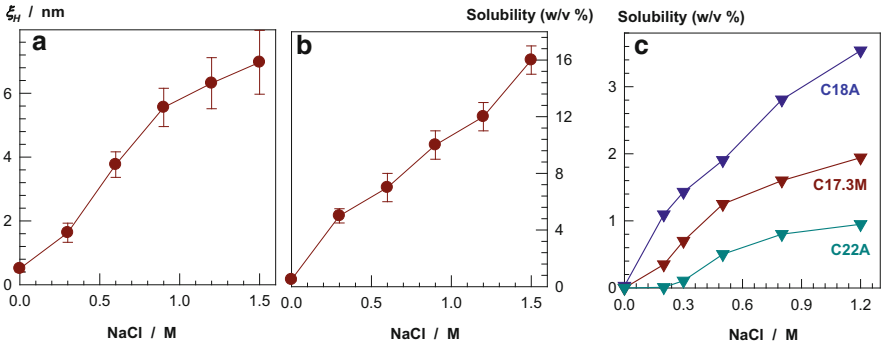

Fig. 3 (**a**) Hydrodynamic correlation length, ξ_H, of a 22 % (w/v) SDS solution and (**b**) solubility of C18A plotted against NaCl concentration; temperature = 55 °C. From [38] with permission from the American Chemical Society. (**c**) Solubilities of C17.3M, C18A, and C22A in surfactant solutions plotted against NaCl concentration; SDS = 7 % (w/v), temperature = 35 °C. From [34] with permission from Elsevier

SDS solution [34, 38]. The hydrodynamic correlation length of the solution, ξ_H (Fig. 3a), and the solubility of C18A (Fig. 3b) are plotted as a function of the NaCl concentration. As the salt concentration is increased, ξ_H also increases, indicating growth of SDS micelles. The micellar growth occurs as a result of transformation of the structure of SDS micelles from spherical to rodlike and then to flexible wormlike micelles [63–67]. Assuming a prolate ellipsoidal shape for the SDS micelles in aqueous NaCl and equating the semi-minor axis with the radius of the minimum-spherical micelle (2.5 nm) [68, 69] allows estimation of the semi-major axis of the micelles using Perrin's equations [70]. The calculations indicate that at 1.5 M NaCl, the major axis between the entanglements becomes 19 ± 4 nm, with corresponding aggregation numbers of 450 ± 100, as compared with only 60 for the minimum-spherical SDS micelle.

The growth of SDS micelles is accompanied by increased solubilization of hydrophobes. As seen in Fig. 3b, the solubility of the C18A monomer in a micellar solution increases from 0 to 16 % (w/v) as the salt concentration increases from 0 to 1.5 M [38]. Figure 3c shows the solubility of three different hydrophobes in 7 % (w/v) SDS solution plotted against the additional-NaCl concentration [34]. The increase in solubility as a result of salt addition is the largest for C18A monomer, followed by C17.3M and C22A. Although the average alkyl side chain of C17.3M is shorter than that of C18A, the methacrylate group of the former molecule seems to be responsible for its lower solubility in the micellar solution. After addition of the monomers to the solution of grown micelles, the hydrodynamic correlation length ξ_H decreases again due to the oil-induced structural change of the wormlike micelles [32, 33, 42]. Even visual inspection of the micellar solutions provides evidence that solubilization of the monomers reduces the viscosity. This change probably occurs as a result of accumulation of monomers in the surfactant palisade layer and in the core of the micelles, which increases the curvature of the micelles and leads to a rod–sphere transition of the micellar shape [71–75].

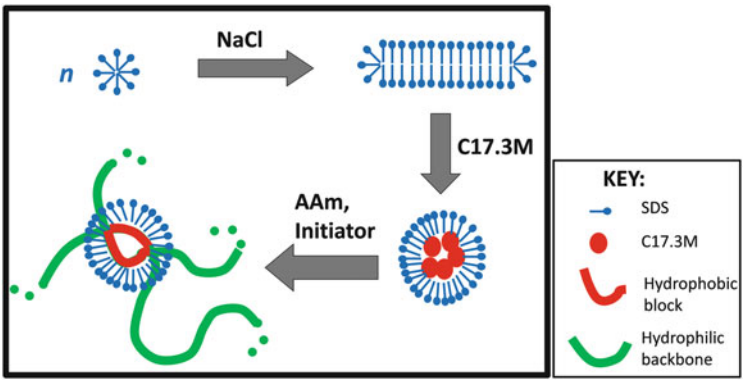

Fig. 4 Preparation of physical PAAm hydrogels in aqueous solutions of SDS–NaCl via hydrophobic C17.3M blocks. From [33] with permission from the American Chemical Society

An alternative route to promote micellar growth and, hence, to solubilize large hydrophobes is mixing of cationic and anionic surfactants. Aqueous solutions of surfactants of opposite charges, called catanionic surfactants, exhibit unique properties originating from the strong electrostatic interactions between their oppositely charged head groups. Mixtures of the anionic surfactant SDS and the cationic surfactant CTAB form mixed micelles in both SDS-rich and CTAB-rich solutions, whereas between these compositions, vesicles and formation of a 1:1 precipitate are observed [76–79]. It was shown that the correlation length of 0.24 M CTAB–SDS increases from 0.4 to 2.5 nm as the SDS content of the surfactant mixture is increased from 0 to 15 mol%, leading to increased solubility of the hydrophobic monomer C17.3M in the micellar solution [37].

After solubilization of large hydrophobes within the wormlike surfactant micelles of salt solutions, they can be copolymerized with hydrophilic monomers to obtain physical gels with tunable properties (Fig. 4). The following sections focus on the properties of hydrogels formed via micellar polymerization in the absence of any chemical cross-linker; hybrid gels formed by both covalent and noncovalent cross-links are not reviewed. If not otherwise indicated, the mole fraction of the hydrophobic monomer in the comonomer feed (f_{HM}) is 0.02; that is, the hydrophilic chains of the hydrogels discussed below contain about 2 mol% of hydrophobic units forming intermolecular hydrophobic associations. They were mainly prepared in 0.5 M NaCl solutions of 7 % (w/v) SDS, in which the aggregation number of SDS micelles is 200 [32].

3 Microstructure of the Network Chains

Polymer hydrogels formed via hydrophobic interactions of large hydrophobes such as C17.3M, C18A, or C22A are insoluble in water, with a gel fraction close to unity. This indicates the existence of strong associations between the hydrophobic blocks

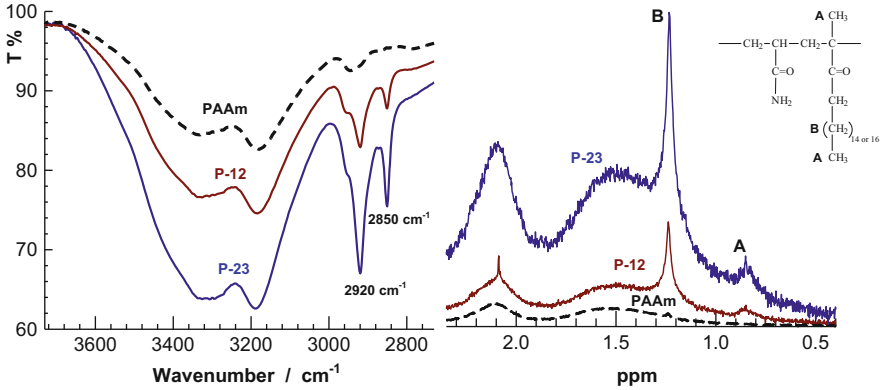

Fig. 5 FTIR (*left*) and ^{1}H NMR (*right*) spectra of HM PAAm network chains (P-12 and P-23) together with spectra of unmodified PAAm. P-12 and P-23 denote the polymers isolated from hydrogels with $N_H = 12$ and 23, respectively. The inset to the figure shows the structure of HM PAAm. The peaks denoted by A and B in NMR spectra arise due to the protons indicated in the inset. From [34] with permission from Elsevier

that cannot be destroyed during expansion of the polymer network in water. However, the networks can be dissolved in solutions of surfactant or in DMSO at high temperatures, which allows microstructural characterization of the polymers. In this section, typical results are reported for hydrophobically modified polyacrylamide (HM PAAm) hydrogels prepared using 2 mol% of C17.3M [34]. The blockiness of the polymer chains was demonstrated using physical gels synthesized at two different initial monomer concentrations (C_0),5 % and 10 % (w/v). Because the aggregation number of SDS micelles in 0.5 M NaCl solution is 200, the length of the hydrophobic blocks in the polymer chains, N_H, is 12 and 23 for hydrogels prepared at $C_0 = 5$ and 10 % (w/v), respectively [34]. Polymers isolated from hydrogels with $N_H = 12$ and 23 are designated P-12 and P-23, respectively.

FTIR and ^{1}H NMR spectra of HM and unmodified PAAm chains are shown in Fig. 5 [34]. In these FTIR spectra, HM PAAm network chains (P-12 and P-23) show characteristic peaks at 2,920 cm^{-1} and 2,850 cm^{-1} caused by the stretching vibrations of CH_2 groups of the C17.3M units. These peaks are absent in unmodified PAAm (dashed curve in Fig. 5). ^{1}H NMR spectra of HM PAAm dissolved in d_6-DMSO exhibit characteristic signals arising from the C17.3M units. In Fig. 5, peak A at 0.9 ppm corresponds to the protons of the α-methyl backbone and the terminal methyl of the alkyl chain, whereas peak B at 1.2 ppm is a result of the protons attached to carbon atoms on the alkyl side chain of the C17.3M units. Although NMR is not sensitive enough to determine the copolymer microstructure because of the low hydrophobe content (2 mol%), the increasing peak intensities with increasing N_H indicate blockiness of the polymers.

To demonstrate the associativity of the network chains, viscosity and rheological measurements were performed on HM PAAms dissolved in 0.7 % SDS solutions. These measurements also show a strong enhancement of the associativity with increasing N_H (i.e., with increasing length of the hydrophobic blocks) [34]. Figure 6a shows the dependence of the viscosity of 0.5 % (w/v) solutions of HM and

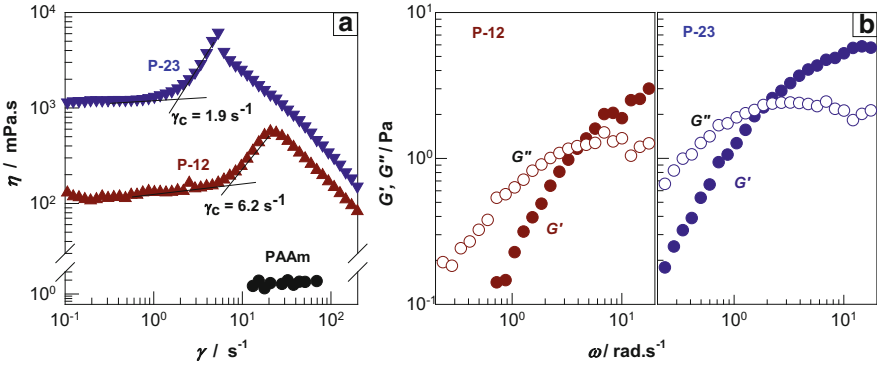

Fig. 6 (**a**) Shear-rate dependence of the viscosity and (**b**) frequency-sweeps of the elastic (G') and viscous (G'') shear moduli for solutions of P-12, P-23, and PAAm; polymer = 0.5 % (w/v), SDS = 0.7 % (w/v), NaCl = 0.5 M, temperature = 35 °C. From [34] with permission from Elsevier

unmodified PAAm on the shear rate. A significant increase in the viscosities of HM PAAm solutions (P-12 and P-23) compared with PAAm solution illustrates the existence of hydrophobic blocks in the network chains. The solutions of P-12 and P-23 exhibit a Newtonian plateau at low shear rates, followed by an abrupt shear thickening region before the onset of shear thinning. The shear thickening region is characteristic for associative flexible polymers and appears as a result of intermolecular hydrophobic associations [80–82]. Although these associations are favorable at a certain degree of coil deformation, they are disrupted at higher shear rates. The critical shear rate for the onset of shear thickening (γ_c) leads to a characteristic time, $\tau_c = 1/\gamma_c$, scaling with the zero-shear viscosity, which is verified by the data in Fig. 6. For P-23 and P-12 solutions, τ_c is 0.53 and 0.16 s, with zero-shear viscosities of 1.18 and 0.11 Pa s, respectively. Thus, despite the same hydrophobe level, solutions of P-23 ($N_H = 23$) exhibit longer τ_c and higher viscosities than solutions of P-12 ($N_H = 12$), demonstrating increasing associativity of the polymers as a result of the increasing length of their hydrophobic blocks. These results are also confirmed by frequency-sweep tests (Fig. 6b). The characteristic relaxation times (τ_R) calculated from the cross-over frequency (ω_c) at which G' and G'' are equal ($\tau_R = \omega_c^{-1}$) are 0.31 and 0.53 s for P-12 and P-23 solutions, respectively. This finding also reveals strong associativity of the network chains of the physical gels described.

4 Swelling Properties

Figure 7a shows typical swelling kinetics of HM PAAm hydrogels where the relative gel mass in water (m_{rel}) is plotted against the swelling time [33]. In Fig. 7b, the amount of SDS released from the gel is plotted as a function of the swelling time. As a result of the osmotic pressure of SDS counterions within the

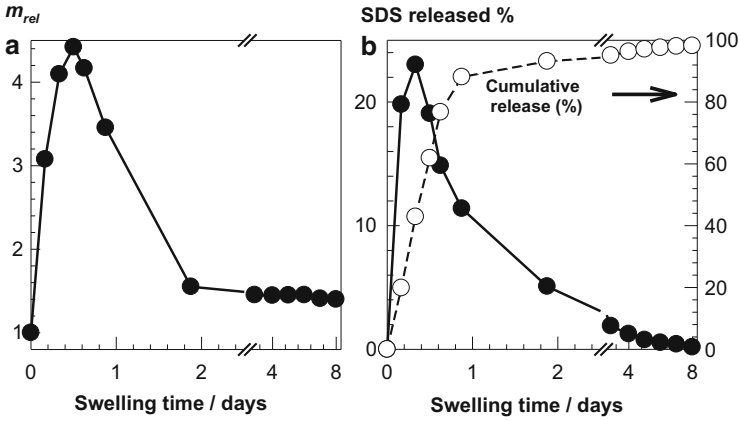

Fig. 7 (**a**) Relative weight swelling ratio (m_{rel}) of HM PAAm hydrogel formed in 7 % (w/v) SDS + 0.5 M NaCl solution and (**b**) released amount of SDS from the hydrogel, both shown as a function of the time of swelling in water; $C_0 = 10$ %, C17.3M = 2 mol%. From [33] with permission from the American Chemical Society

hydrogel, the gel initially behaves like an ionic gel and, therefore, attains a large swelling ratio m_{rel}. However, as the surfactant is gradually released from the hydrogel, the osmotic effect vanishes and the hydrogel progressively changes into a nonionic hydrogel with a distinctly reduced swelling ratio. The cumulative SDS release data in Fig. 7b reveal that all SDS was extracted from the gels after a swelling time of 8 days. Indeed, sulfur analysis of freeze-dried gel samples revealed no sulfur, indicating complete SDS extraction [33]. The swelling measurements carried out in aqueous salt solutions confirm this interpretation of the course of the swelling curves [33]. NaCl addition to the external solution reduces the swelling degrees at short times as a result of reduction of the osmotic pressure difference between the inside and outside of the hydrogel. The maximum of the swelling curves totally disappears if the salt concentration in the external solution approaches the counterion concentration in the hydrogel.

The swelling kinetics of hydrophobically modified nonionic hydrogels such as HM PAAm and HM poly(*N*,*N*-dimethylacrylamide) (PDMA) prepared in salt solutions of SDS, CTAB, or CTAB–SDS are similar to those illustrated in Fig. 7 [37, 41]. In contrast, HM PAAc hydrogels formed in SDS solutions exhibit high swelling ratios in water because of the osmotic pressure of the AAc counterions [39]. The equilibrium swelling ratio ($m_{rel,eq}$) of these hydrogels formed at $C_0 = 20$ % (w/v) is around 500, corresponding to a PAAc concentration of 0.04 % (w/v) in the swollen gel. Even at such a high degree of dilution, the hydrophobic associations acting as physical cross-links of the highly stretched PAAc network remain stable in equilibrium with water.

A completely different swelling behavior is observed for ionic hydrogels formed in solutions of oppositely charged surfactants. Figure 8a, b shows m_{rel} of HM PAAc hydrogels formed in CTAB–NaBr solutions plotted against the swelling time in

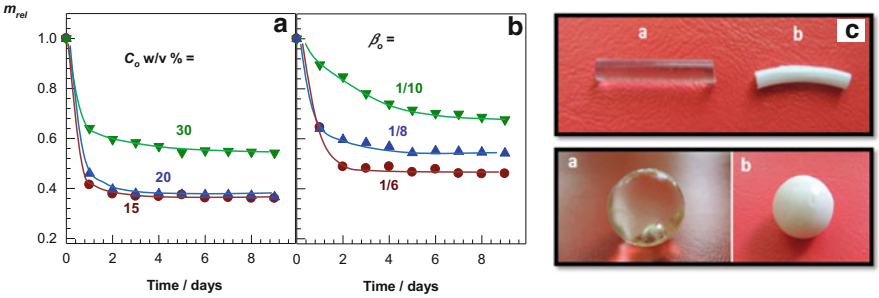

Fig. 8 (**a**, **b**) Relative mass (m_{rel}) of HM PAAc gels formed at a CTAB/AAc ratio (β_0) in the feed of 1/8 (**a**) and at C_0 of 30 % (w/v) (**b**) plotted against the swelling time in water. (**c**) Photographs of HM PAAc hydrogels after preparation (*a*) and in equilibrium with water (*b*); $C_0 = 20$ % (w/v), C17.3M = 2 mol%, $\beta_0 = 1/8$, NaBr = 0.25 M. From [42] with permission from the American Chemical Society

water [42]. The hydrogels deswell in water, with 40–60 % reduction of the gel mass as a result of the onset of complexation between PAAc and CTAB upon immersion in water. Indeed, polymers isolated from hydrogels that were in thermodynamic equilibrium with pure water contained nitrogen, indicating the presence of polymer-bound CTAB molecules. It was shown that, on average, 8–15 AAc units of the physical network carry CTA counterions that cannot be extracted with water [42]. The CTAB/AAc ratio (β) of the polymer increases as the CTAB/AAc ratio in the feed (β_0) is increased or as the initial monomer concentration (C_0) is decreased. The increase in β also leads to a more collapsed state of the gels in water, as seen in Fig. 8a, b. Because the pH inside the hydrogel after its preparation is equal to 1.5, PAAc is mostly protonated, so that no complexes form between PAAc and CTAB. However, upon immersion in water, the pH increases to 6.7, leading to ionization of the AAc units and, hence, to the onset of complexation [83, 84]. The formation of PAAc–CTAB complexes is also obvious from inspection of the gel samples (Fig. 8c): the hydrogels that are transparent after preparation become opaque in water, and the opacity increases with the β ratio [42].

5 Dynamics of Hydrogels With and Without Free Surfactant Micelles

Hydrogels formed via hydrophobic interactions in aqueous micellar solutions present two faces, depending on their state, namely:

1. The state of preparation, in which they contain surfactant micelles
2. The state of equilibrium in pure water, where free surfactant micelles have been removed

This section summarizes the dynamic properties of hydrophobically modified hydrogels in both these states. Those hydrogel systems forming no complexes with surfactants are mainly discussed, including PAAm, PDMA, or PAAc hydrogels, all formed in SDS solutions. Hydrogels capable of forming complexes with surfactants, such as polyelectrolyte hydrogels formed in solutions of oppositely charged surfactants, are discussed later in this section. Moreover, for a better understanding of the dynamics of these complex aqueous systems composed of surfactant micelles, salts, hydrophobic associations, and hydrophilic polymer chains, the dynamics of the hydrogels are also compared to those of the surfactant solutions.

Dynamic light scattering (DLS) is a powerful tool for investigating the associative and aggregation phenomena in polymer solutions and gels. DLS measurements on hydrogels formed by hydrophobic associations have been reported at various preparation steps of the gelation solutions: before and after addition of salt and monomers to the surfactant solution, after micellar copolymerization, and after removal of surfactant micelles from the hydrogels [32, 33, 37]. Figure 9a, b shows typical time-average intensity correlation functions (ICFs) obtained at a scattering angle (θ) of $=90°$ from SDS solutions and HM PAAm hydrogels, respectively [33]. The ICF of the 7 % SDS solution shows both fast and slow relaxation modes (Fig. 9a). These relaxations merge into just one after addition of salt and the monomers C17.3M and AAm to the surfactant solution, leading to disappearance of the slow mode. After formation of physical HM PAAm hydrogels, a slow mode appears again on an even longer time scale (Fig. 9b). However, when the surfactant micelles are removed from the hydrogels, the slow mode disappears.

The scattering-vector dependencies of the relaxation rates give additional information on the dynamic properties of the physical gels [33]. In Fig. 9c, d, the relaxation rates of the fast (Γ_{fast}) and slow modes (Γ_{slow}) calculated from the peak positions in the relaxation-rate distribution functions, $G(\Gamma)$, are plotted against the square of the scattering vector, $q = (4\pi n/\lambda)\sin(\theta/2)$, with n being the refractive index of the solvent and $\lambda = 633$ nm. Both fast and slow relaxation modes for SDS solutions in water are proportional to q^2, indicating diffusive processes. The hydrodynamic correlation length (ξ_H) based on the fast mode is 0.5 nm for SDS micelles in water, but after NaCl addition, it increases to 6.1 nm due to formation of wormlike micelles [32, 33, 69, 85]. Addition of C17.3M and AAm to the SDS–NaCl solution re-decreases ξ_H to 3 nm as a result of an oil-induced structural change of the wormlike micelles [32, 33, 42]. In contrast to the slow mode of the SDS solution, the slow mode of HM PAAm hydrogels containing SDS (~30 ms) is independent of q (filled symbols in Fig. 9d). This reveals that the slow mode of the hydrogels is associated with the structural relaxation of the physical PAAm hydrogels on a time scale of milliseconds. This relaxation takes place if the surfactant micelles are present within the gel network whereas it vanishes in the absence of surfactants.

The internal dynamics of the physical hydrogels formed by hydrophobic associations was also investigated by rheological tests. In Fig. 10a–c, the elastic modulus, G' (filled symbols), the viscous modulus, G'' (open symbols), and the loss factor $\tan\delta$ (G''/G'; lines) of HM PAAm hydrogels with and without SDS are

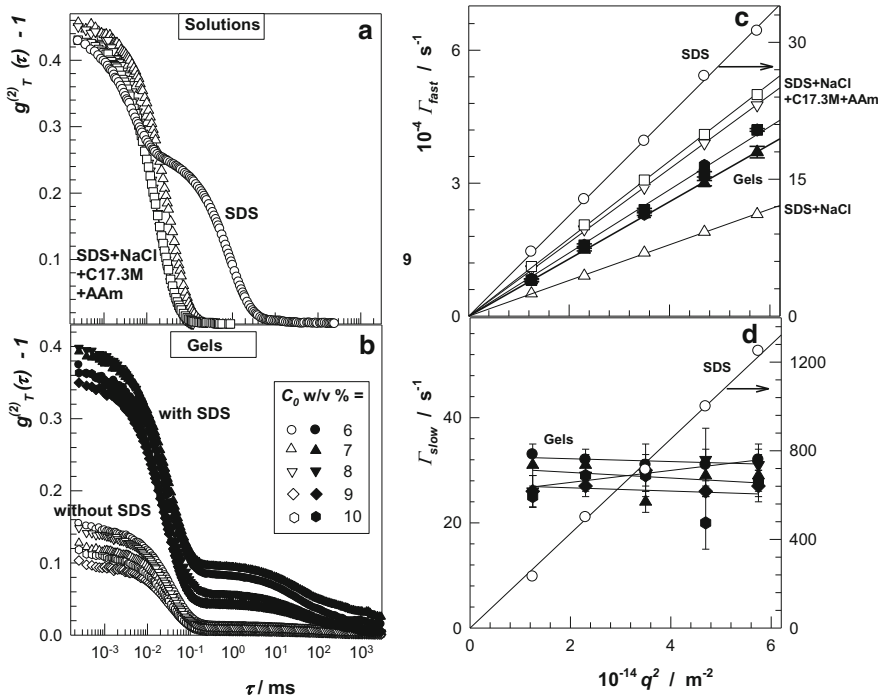

Fig. 9 (**a**, **b**) Intensity correlation functions (ICFs) of SDS solutions (**a**) and HM PAAm hydrogels (**b**), recorded at a detection angle of $\theta = 90°$. Data are shown for solutions of SDS without (*open circles*) and with NaCl (*open up-triangles*), NaCl + C17.3M (*open down-triangles*), and NaCl + C17.3M + AAm (*open squares*). C17.3M and AAm concentrations correspond to the synthesis recipe of a hydrogel at $C_0 = 10$ % (w/v). *Filled* and *open symbols* in (**b**) show data for hydrogels with and without SDS, respectively. (**c**, **d**) Relaxation rates of the fast (Γ_{fast}) (**c**) and slow (Γ_{slow}) (**d**) modes shown as a function of q^2 for hydrogels and solutions probed by these studies. The *symbols* are the same as for (**a**, **b**). From [33] with permission from the American Chemical Society

shown as a function of the angular probe frequency ω [34]. The hydrogels were prepared using three different hydrophobes: C17.3M, C18A, and C22A [34]. The dynamic moduli of the hydrogels containing SDS are dependent on time, with a plateau region at high frequencies (10^2 rad s^{-1}), and they exhibit a loss factor, tan δ, above 0.1. This result reveals the temporary nature of the associations, with lifetimes of the order of seconds to milliseconds. Upon removal of the surfactant, the elastic moduli become nearly independent of time, and tan δ decreases below 0.1, revealing formation of a strong hydrogel with negligible viscous properties. The drastic change in the dynamics of this gel is a result of the strengthening of the hydrophobic associations in the absence of surfactant micelles, so that the dynamic behavior approaches that of conventional chemically cross-linked hydrogels.

Thus, in the presence of SDS micelles, the cross-links are reversible because of the local solubilization of the hydrophobic associations. As a consequence, the

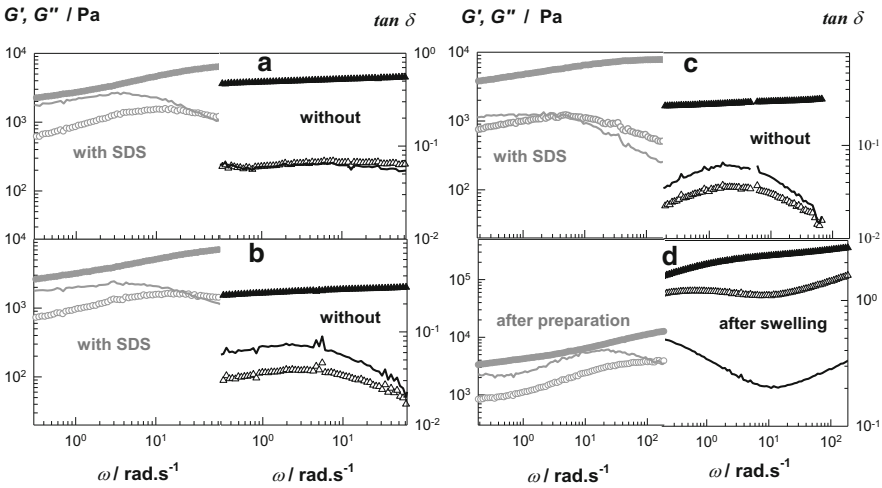

Fig. 10 (**a**–**d**) G' (*filled symbols*), G'' (*open symbols*), and tan δ (*lines*) of hydrophobically modified hydrogels shown as a function of the angular probe frequency ω; hydrophobe content = 2 mol%, $\gamma_0 = 0.01$. (**a**–**c**) HM PAAm hydrogels with 7 % (w/v) SDS and without SDS; hydrophobe = C17.3M (**a**), C18A (**b**), and C22A (**c**); $C_0 = 10$ % (w/v). From [34] with permission from Elsevier. (**d**) HM PAAc hydrogels formed in CTAB solutions after preparation and after swelling in water; $C_0 = 10$ % (w/v), hydrophobe = C17.3M, $\beta_0 = 1/8$. From [42] with permission from the American Chemical Society

hydrogels containing SDS belong to the category of weak gels. Without surfactant micelles, the lifetime of the hydrophobic associations increases as a result of their direct exposure to the aqueous environment, so that they behave like strong chemical gels, with time-independent moduli and a single relaxation mode in DLS (Fig. 9b). These findings also suggest that the existence of surfactant micelles is responsible for the slow mode of the physical gels. Previous work shows a slow relaxation mode in the micellar kinetics on a time scale of milliseconds to seconds, which corresponds to the dissolution of a micelle into individual surfactant molecules [86]. Because the disintegration of a micelle around the hydrophobic blocks increases the extent of hydrophobic interactions at this site, whereas its re-formation reduces these interactions again, one may expect that the micellar kinetics and resulting transient strong associations are responsible for the slow relaxation mode in physical gels containing surfactant micelles.

The water insolubility of the physical gels formed via hydrophobic interactions, even in a critical gel state [32], is in accord with the above findings. During the swelling process, removal of surfactants from the hydrogels increases the lifetime of the associations, so that the gels become increasingly stable as the surfactant is gradually extracted. By contrast, if swelling is carried out without extraction of the surfactants, the hydrogels should dissolve because of the weak hydrophobic associations. As mentioned in Sect. 3, this was indeed observed. At or above 5 % SDS concentration, HM PAAm hydrogels formed in 7 % SDS solution totally dissolve within 7–21 days. As a result of weakening of the hydrophobic associations with

rising surfactant concentration, physical gels dissolve faster as the SDS amount in the external solution increases.

The rheological behavior of HM PAAc hydrogels formed in CTAB solutions is similar to that of the nonionic hydrogels summarized above, as long as they are probed at a state of preparation (Fig. 10d) [42]. Both moduli of the hydrogels are dependent on frequency, and the loss factor tan δ remains above 0.1 in a range of frequencies between 0.08 and 400 rad s^{-1}. However, upon immersion in water and after extraction of free CTAB micelles, a different behavior is observed. As seen in Fig. 10d, the dynamic moduli of HM PAAc hydrogels increase by one order of magnitude, suggesting the effect of complex formation between PAAc with CTA counterions (Fig. 8). Nevertheless, both moduli of the gel are still dependent on frequency, and tan δ remains above 0.1 in equilibrium with water (i.e., after extraction of free CTAB micelles). This finding emphasizes the viscous character of the HM PAAc hydrogels in aqueous environment as a result of the presence of polymer-bound CTA counterions.

The size of the micelles also affects the dynamics of the hydrogels. This effect was investigated in HM PAAm hydrogels formed in aqueous solutions of CTAB containing 0–15 mol% of SDS [37]. Similarly to the addition of NaCl, addition of SDS–CTAB solution increases the size of the micelles (see Sect. 2). Because an increasing micellar size also increases the number of hydrophobic molecules solubilized in a given micelle (Eq. 1a), the length of the hydrophobic blocks of the hydrophilic network chains can be changed by varying the SDS content of the cationic surfactant solution. Figure 11a shows the frequency dependencies of G' (filled symbols) and G'' (open symbols) for HM PAAm hydrogels formed in 0.24 M CTAB–SDS solutions with varying SDS content [37]. Figure 11b shows the relaxation moduli, $G(t)$, of the same gels in the linear regime as a function of time (t) at different strains (γ_0). The hydrogels show frequency- or time-dependent dynamic moduli, with $G'(\omega)$ being a mirror image of $G(t)$. At time scales spanning two decades (1–100 s), they exhibit a power-law behavior, $G(t) \sim t^{0.31 \pm 0.08}$, as indicated in Fig. 11b by the solid red lines. At times shorter than 1 s, Rouse-type relaxation is seen, which is fitted using a stretched-exponential function, $G(t) = G_R \exp[-(t/\tau_1)^{\beta}]$, with an exponent $\beta = 0.46 \pm 0.04$, where G_R is the Rouse modulus and τ_1 is the lifetime of associations (i.e., the average residence time of a hydrophobic block in a given association, shown by dashed red curves in Fig. 11b) [49, 87–89].

The Rouse modulus, G_R, and the lifetime τ_1 derived from the fits are plotted against the SDS content in Fig. 12 [37]. The elastic moduli of the gels, G'_{ω} at $\omega = 250$ rad s^{-1}, corresponding to an experimental time scale of 4 ms, are also shown in Fig. 12. As the SDS content of the hydrogels is increased (i.e., as the micelles grow), the lifetime of the hydrophobic associations also increases, whereas the modulus G_R or G'_{ω} decreases at short times. These results highlight the effect of the size of the micelles on the length of the hydrophobic blocks. Because the hydrophobe level is fixed (2 mol%, except for the gels formed in CTAB solutions, where it is 1.4 mol%), increasing micellar size also increases the number of C17.3M

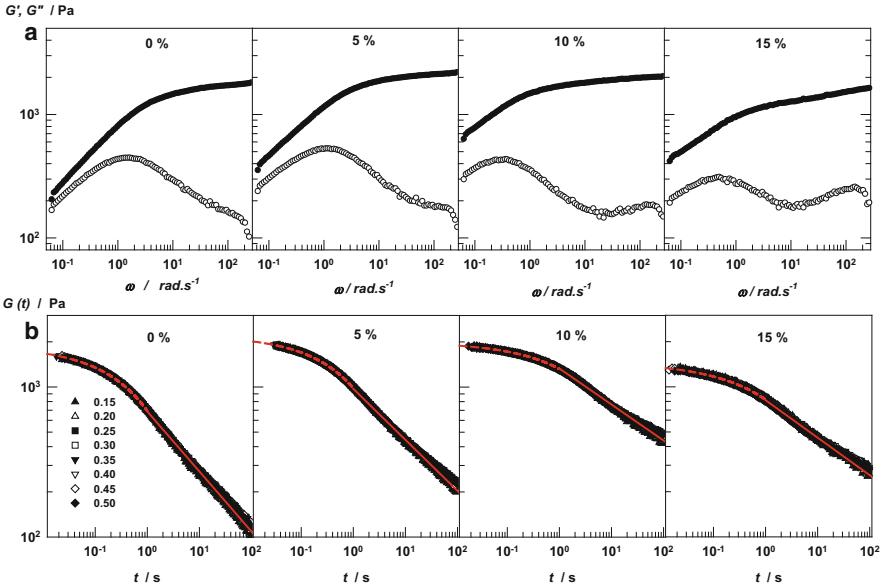

Fig. 11 (**a**) G' (*filled circles*) and G'' (*open circles*) of HM PAAm hydrogels plotted against the angular probe frequency (ω); $\gamma_0 = 0.01$. SDS amounts (mol%) in the gel-formation media, which are CTAB–SDS mixtures, are indicated in the panels; temperature = 35 °C, $C_0 = 5$ % (w/v), C17.3M = 2 mol%, CTAB + SDS = 0.24 M. (**b**) Relaxation modulus, $G(t)$, of the hydrogels plotted against time (t) for strains (γ_0) ranging from 0.15 to 0.50. SDS amounts (mol%) in the gel-formation media are indicated in the panels. From [37] with permission from the Royal Society of Chemistry

molecules solubilized in a given micelle, so that longer hydrophobic blocks form after polymerization, but the number of blocks per primary polymer chain decreases. This increases the lifetime of the associations but decreases their concentration, as evidenced by the Rouse modulus of the physical gels. The lower modulus of the gels formed in the absence of SDS is attributed to the incomplete solubility of C17.3M in the reaction solution, leading to less hydrophobic associations in the final gels.

An experimental proof of this mechanism requires microstructural characterization of the network chains isolated from the physical gels. The hydrogels can be dissolved in CTAB–SDS solutions to prepare a polymer solution [0.5 % (w/v)] having the same concentration and composition of the surfactant mixture as that used for gel preparation [37]. This way, although the gels are solubilized, the surfactant environment of the disintegrated network chains remains unchanged. Figure 13a presents flow curves for 0.5 % (w/v) polymer solutions obtained by this approach from gels made with SDS contents between 0 % and 15 % [37]. The solutions of polymers with 0 % and 5 % SDS show low viscosities, whereas those with 10 % and 15 % SDS exhibit higher viscosities at low shear rates, along with marked shear thinning. Because the increase in the viscosity with rising SDS

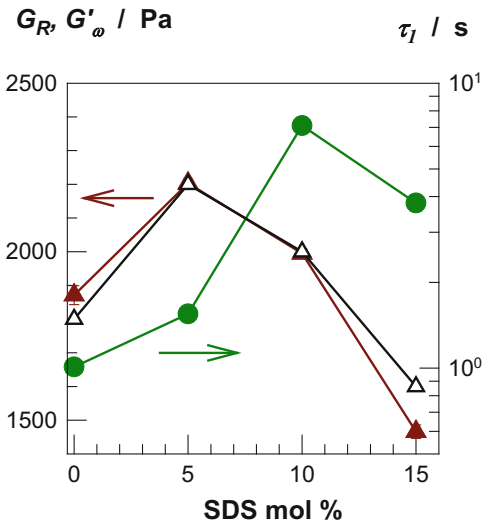

Fig. 12 Rouse modulus, G_R (*filled triangles*), elastic modulus, G'_ω at $\omega = 250$ rad s^{-1} (*open triangles*), and the lifetime τ_1 of hydrophobic associations in HM PAAm hydrogels formed in 0.24 M CTAB–SDS solutions (*filled circles*), plotted against the SDS content. From [37] with permission from the Royal Society of Chemistry

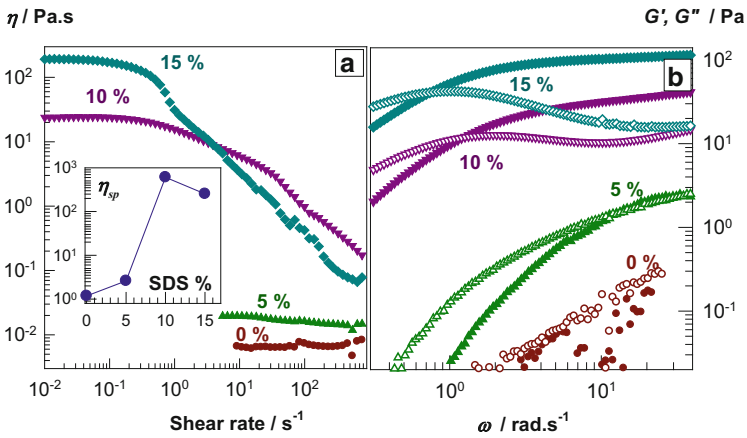

Fig. 13 (**a**) Viscosity versus shear rate and (**b**) frequency sweeps for 0.5 % (w/v) HM PAAm solution in 0.24 M CTAB–SDS solutions. The SDS amounts (in mol%) of CTAB–SDS mixtures are indicated. In (**b**), the elastic modulus G' and viscous modulus G'' are shown by *filled* and *open symbols*, respectively. *Inset* to (**a**) shows the specific viscosity, η_{sp}, of polymer solutions plotted against their SDS content; temperature = 35 °C. From [37] with permission from the Royal Society of Chemistry

content can be attributed to micellar growth rather than to the increasing associativity of polymers, the viscosities of the surfactant solutions without polymers were also measured. The relative viscosity increase as a result of the polymer is represented as the specific viscosity, η_{sp}, defined as $\eta_{sp} = \eta_{0,polymer}/\eta_{0,solvent} - 1$, where $\eta_{0,polymer}$ and $\eta_{0,solvent}$ are the zero-shear viscosities of CTAB–SDS solutions with and without polymers. The inset to Fig. 13a shows the specific viscosity η_{sp} of polymer solutions plotted against their SDS content. The value of η_{sp} sharply increases with rising SDS content, indicating increasing associativity of the network chains as the amount of SDS present during gel preparation is increased.

In Fig. 13b, the dynamic moduli G' and G'' of HM PAAm solutions are plotted against the angular probe frequency. The characteristic relaxation times (τ_R) calculated from the cross-over frequencies at which the G' and G'' curves intersect (ω_c) are 0.09, 0.83, and 1.3 s for SDS contents of 5, 10, and 15 mol%, respectively. This finding indicates increasing associativity of the polymer chains with increasing content of SDS in the gel system. Figure 13b also shows that at 5 % SDS, a distinct plateau appears in G' at high frequencies. The height of this plateau increases and its width enlarges with increasing amounts of SDS. For HM PAAm solution containing 15 % of SDS, the elastic modulus at the plateau is two orders of magnitude higher than that for the polymer solution with just 5 %. Thus, the polymers prepared in CTAB–SDS solutions with 10 % and 15 % of SDS show remarkable associativity. This effect can be attributed to the noticeable blockiness of the polymer chains and to the increasing size of the wormlike CTAB micelles around the hydrophobic blocks.

6 Structural Inhomogeneity

Polymer gels are known to exhibit pronounced scattering of light, neutrons, and X-rays at low scattering vectors, corresponding to concentration fluctuations at length scales between 10^0 and 10^2 nm [90, 91]. Such large-scale concentration fluctuations, which are absent in polymer solutions, are a result of the mesoscopic static structures in gels, called the spatial gel inhomogeneity [90–94]. This inhomogeneity can be visualized as strongly cross-linked nanogel clusters embedded in a less densely cross-linked environment. Because the gel inhomogeneity results in a drastic reduction in the mechanical performance of hydrogels and is thus undesirable in many gel applications, preparation of homogeneous gels is a challenging task. As the gel inhomogeneity is connected to the spatial concentration fluctuations, it is widely investigated using scattering methods such as DLS. This technique provides the time-average intensity correlation function, $g_T^{(2)}(q,\tau)$, whose short-time limit is related to an apparent diffusion coefficient, D_A, via [95, 96]:

$$D_A = -\frac{1}{2q^2}\lim_{\tau\to 0}\ln\left(g_T{}^{(2)}(q,\tau) - 1\right) \tag{2}$$

where τ is a decay time. For a nonergodic system containing an infinite network such as polymer gels, D_A and the time-averaged scattering intensity $<I(q)>_T$ fluctuate randomly with the sample position. $<I(q)>_T$ has two contributions: one from static inhomogeneities (frozen structure) and another from dynamic fluctuations, as represented by the following equation [95–97]:

$$\langle I(q)\rangle_T = I_C(q) + \langle I_F(q)\rangle_T \tag{3}$$

where $I_C(q)$ and $<I_F(q)>_T$ represent the scattered intensity as a result of static inhomogeneity and dynamic fluctuations, respectively. By applying the partial heterodyne approach [95], $<I(q)>_T$ can be separated into its two parts:

$$\frac{\langle I(q)\rangle_T}{D_A} = \frac{2\langle I(q)\rangle_T}{D} - \frac{\langle I_F(q)\rangle_T}{D} \tag{4}$$

where D is a cooperative diffusion coefficient related to the dynamic correlation length by $\xi = kT/(6\pi\eta D)$, with η the viscosity of the medium and kT the Boltzmann thermal energy. Equation (4) applies to each sample position. Thus, for different sample positions, different D_A and $<I(q)>_T$ are obtained. Using DLS measurements conducted at different sample positions together with Eq. (4), one may calculate the cooperative diffusion coefficient D and the dynamic part of the scattering intensity $<I_F(q)>_T$.

Figure 9b shows a significant decrease in the initial amplitude of the ICF upon removal of the surfactant from HM PAAm hydrogels, indicating an increasing extent of frozen concentration fluctuations. Figure 14a shows the time-averaged

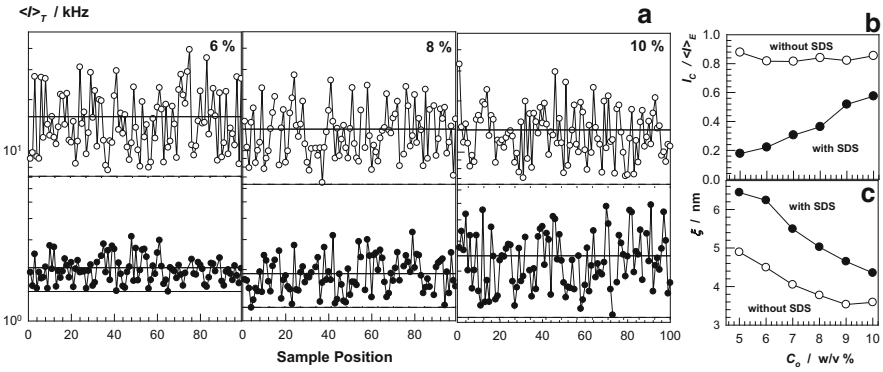

Fig. 14 (**a**) $<I>_T$ at various sample positions for HM PAAm hydrogels formed using 2 mol% of C17.3M with 7 % (w/v) of SDS (*filled circles*) and without SDS (*open circles*). C_0 is indicated in the panels. (**b**, **c**) C_0 dependences of $I_C/<I>_E$ (**b**) and ξ (**c**). From [33] with permission from the American Chemical Society

scattering intensity $<I>_T$ at $\theta = 90°$ for randomly chosen sample positions within HM PAAm gels with 7 % (w/v) of SDS (filled symbols) and without SDS (open symbols) [33]. The solid lines in Fig. 9b represent the ensemble-averaged scattering intensity, $<I>_E$, obtained by averaging $<I>_T$ over many sample positions. The dashed lines represent that part of the scattering intensities $<I_F>_T$ that is due to liquid-like concentration fluctuations. It is seen that the removal of surfactant from the hydrogels results in an almost one order of magnitude increase in the spatial fluctuations in $<I>_T$. To capture the spatial gel inhomogeneity, the relative contribution of the static component (frozen structure) of the scattered intensity, $I_C/<I>_E$, is plotted against C_0 in Fig. 14b. A considerable portion of the thermal scattering from the surfactant-containing gels is due to the presence of large SDS micelles; $I_C/<I>_E$ monotonically increases from 20 % to 60 % with rising C_0 as a result of suppression of the fluctuations by the polymer chains. Without surfactant, $I_C/<I>_E$ of the hydrogels is independent of C_0 and equals 83 ± 3 %. Thus, the degree of spatial gel inhomogeneity considerably increases after extraction of the surfactant molecules. This increase is possibly related to a loss of reversibility of the cross-linkages and a resulting increase in the apparent cross-linking density of the gels at long experimental time scales. In Fig. 14c, the correlation length ξ of the gels based on their fast modes is plotted against C_0. The value of ξ of the surfactant-containing gels decreases slightly from 6 to 4 nm, indicating a decreasing gel-network mesh size with rising C_0; it further decreases after extraction of the SDS micelles.

7 Mechanical Properties

Uniaxial compression and tensile measurements on hydrophobically modified hydrogels serve to evaluate their elastic properties such as moduli, fracture stresses, and deformation ratios at break [33–35, 39–42]. The stress is presented by its nominal, σ_{nom}, or true values, σ_{true} (equal to $\lambda\sigma_{nom}$), defined as the forces per unit undeformed and deformed area, respectively; λ is the deformation ratio. Cyclic mechanical tests are powerful tools for investigating the large-strain properties and the reversible nature of cross-links of physical gels. These tests are carried out by stretching or compressing hydrogel samples at a constant cross-head speed to a predetermined maximum load below failure, followed by immediate retraction to zero displacement. After a fixed wait time, the cycles are repeated several times. As no standard method exists to evaluate the self-healing abilities of hydrogels, healing of cylindrical samples after being cut in half is monitored as a function of the healing time in closed containers to prevent water evaporation [33]. The healing efficiency is calculated from the mechanical properties of the virgin and healed gel samples.

Typical compressive stress–strain curves of surfactant-containing hydrophobically modified hydrogels are shown in Fig. 15a, where σ_{nom} and σ_{true} are plotted against the deformation ratio λ [41]. The results obtained from 15 separate HM PDMA hydrogel samples at a state of preparation are presented. The

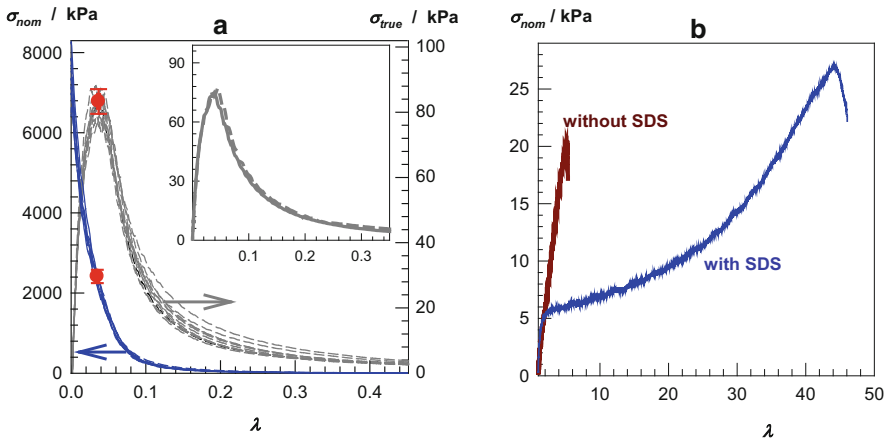

Fig. 15 (**a**) Typical stress–strain curves of a surfactant-containing HM PDMA hydrogel formed using 2 mol% of C17.3M under compression, represented as the dependences of nominal σ_{nom} (*blue solid curves*) and true stresses σ_{true} (*gray dashed curves*) on the deformation ratio λ; SDS = 7 % (w/v). Results of 15 separate tests are shown. *Red circles* represent the points of failure of the gel samples. The *inset* shows σ_{true} versus λ curves of two successive tests conducted on the same gel sample for up to 99.99 % compression. (**b**) Stress–strain curve of the same HM PDMA hydrogel with 7 % (w/v) of SDS (*solid blue curve*) and without SDS (*solid dark red curve*); C_0 = 15 % (w/v), C17.3M = 2 mol%, NaCl = 0.5 M. From [41] with permission from Elsevier

samples do not break, even at a strain of about 100 % compression and, therefore, the nominal stress σ_{nom} increases continuously with increasing strain (solid curves in Fig. 15a). However, the corresponding σ_{true} versus λ plots pass through maxima, indicating the onset of failure in the gel specimen (gray dashed curves in Fig. 15a). The fracture nominal stress and stretch at failure (λ_f), calculated from the maxima in the σ_{true} versus λ plots, are 2.4 ± 0.2 MPa and 0.04 (96 % compression), respectively [41]. However, successive compression tests conducted on the same gel sample show that this failure is recoverable in nature. This is illustrated in the inset to Fig. 15a, where two successive test results are given. Good superposition of the stress–strain curves indicates that the damage in the hydrogel is self-healed upon unloading. The results reveal that the gel can be compressed up to about 100 % strain without any permanent failure. This is a typical behavior of surfactant-containing hydrogels formed via hydrophobic associations. Next, the fracture nominal stress and stretch at failure are reported from the maxima in σ_{true} versus λ plots.

Figure 16a represents stress–strain data of surfactant-containing HM PAAm hydrogels; seven different hydrophobes with linear alkyl side chains of 12–22 carbon atoms were used in their synthesis [34]. In compression tests ($\lambda < 1$), λ at fracture is 0.04, indicating that all these hydrogels are mechanically stable up to 96 % compression. In elongation tests ($\lambda > 1$), λ at break is larger than 16, meaning that the elongation at break is above 1,500 % for these HM PAAm hydrogels. The tensile strength of the hydrogels prepared using hydrophobic acrylates is larger (30–

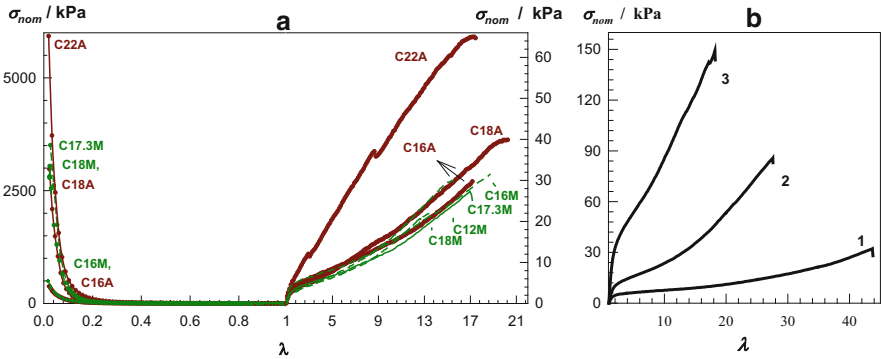

Fig. 16 (**a**, **b**) Stress–strain curves of HM PAAm (**a**) and HM PAAc hydrogels (**b**) after preparation in 7 % SDS + 0.5 M NaCl solutions; hydrophobe content = 2 mol%. (**a**) $C_0 = 10$ % (w/v). From [34] with permission from Elsevier. (**b**) Hydrophobe C17.3M; $C_0 = 15$ % (*1*), 20 % (*2*), and 30 % (*3*). From [39] with permission from the Royal Society of Chemistry

65 kPa) than that of those formed using methacrylates (20–30 kPa). This is a result of the restricted mobility of the methacrylate backbones, reducing the number of hydrophobic associations acting as physical cross-links [34].

In addition to the alkyl side chain length of the hydrophobes, the type of hydrophilic chains also affects the mechanical performance of hydrogels formed via hydrophobic interactions. For instance, replacing PAAm by a PAAc backbone leads to mechanically stronger hydrogels as a result of stabilization of the hydrophobic associations by cooperative hydrogen bonding between the PAAc carboxyl groups [39]. Figure 16b represents tensile stress–strain data of surfactant-containing HM PAAc hydrogels formed at three different concentrations (C_0). At $C_0 = 15$ % (curve 1 in Fig. 16b), the gel withstands 41 ± 11 kPa stresses, and the fracture stress further increases up to 173 ± 33 kPa if C_0 is increased [39]. The stretch at break (λ_f) of the hydrogels is between 19 and 51 (1,800–5,000 % elongation), which is a decreasing function of C_0. Similar improvement of the mechanical performance was observed by replacement of PAAm with a PDMA backbone (solid curve in Fig. 15b). A HM PDMA hydrogel with 7 % (w/v) of SDS ruptures when stretched to 43 ± 4 times its original length, corresponding to $4{,}200 \pm 400$ % elongation [41]. By contrast, PAAm hydrogels formed under identical conditions exhibit elongation at break of only about 2,000 % [33, 34]. This suggests that the hydrogen bonding and hydrophobic interactions between the DMA units additionally contribute to the mechanical properties of these gels.

The results of the mechanical tests presented so far were obtained from hydrogels just after preparation (i.e., from surfactant-containing hydrogels). Because the dynamic features of the hydrogels formed via hydrophobic interactions drastically change after removal of surfactant micelles, similar changes were observed in their mechanical properties. In Fig. 17a, the stress relaxation data of HM PAAm hydrogels with and without SDS are shown in form of the variation of the relaxation modulus of the gels, $G(t)$, with increasing strain at fixed times

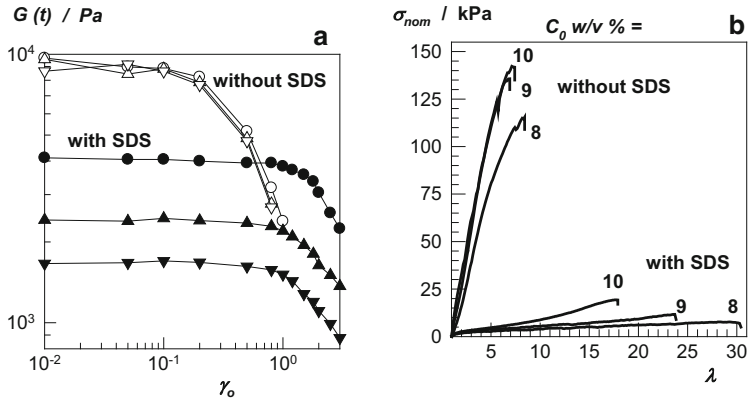

Fig. 17 (**a**) Relaxation modulus $G(t)$ plotted against strain (γ_0) for various times (t) for HM PAAm hydrogels with 7 % (w/v) of SDS (*filled symbols*) and without SDS (*open symbols*); $t = 0.1$ (*circles*), 1.0 (*triangles up*), and 10 s (*triangles down*); $C_0 = 10$ % (w/v), C17.3M = 2 mol%, NaCl = 0.5 M. (**b**) Stress–strain curves of HM PAAm gels with 7 % (w/v) of SDS and without SDS formed at $C_0 = 8$–10 % (w/v), as indicated on the curves; C17.3M = 2 mol%, NaCl = 0.5 M. From [33] with permission from the American Chemical Society

[33]. For surfactant-containing hydrogels, the linear viscoelastic regime extends up to approximately 100 % strain, whereas it is restricted to strains up to ~10 % for surfactant-free hydrogels. This difference shows a significant decrease in the stretchability of these hydrogels upon removal of surfactant [33, 40]. Figure 17b represents tensile stress–strain data of HM PAAm hydrogels prepared at three different concentrations (C_0). With SDS, the elongation at break exceeds 1,700 %, and it increases further as C_0 is decreased. Without SDS, however, the hydrogels break at about 700 % strain and exhibit an order of magnitude larger ultimate strength than the SDS-containing gels. Highly stretchable HM PDMA hydrogels also become brittle after extraction of SDS micelles, and the elongation ratio at break decreases from 43 ± 4 to 5 ± 1 (dark red curve in Fig. 15b) [41].

The amount of surfactant within the hydrogels also affects their mechanical properties [34]. This is illustrated in Fig. 18 for HM PAAm hydrogels where the tensile moduli, the ultimate strength, the elongation at break, and toughness are summarized for samples containing various amounts of SDS. Enhancement of the mechanical strength is seen when the SDS content is decreased, becoming dramatic between 1 % and 0 % of SDS. Hydrogels without SDS exhibit high moduli (~50 kPa), high ultimate strength (~200 kPa), and high toughness (~1 MJ m^{-3}) because of the increased lifetime of hydrophobic associations in the absence of SDS (Fig. 10). The elongation at break decreases from 1,600 % to 800 % as the amount of SDS in the hydrogels is decreased. These results demonstrate that the mechanical properties of the physical hydrogels can be tuned by varying their SDS content.

Ionic hydrogels formed in oppositely charged surfactant solutions exhibit a significant enhancement of their mechanical properties when they are immersed in water [42]. For instance, Fig. 19 shows the stress–strain data of HM PAAc gels

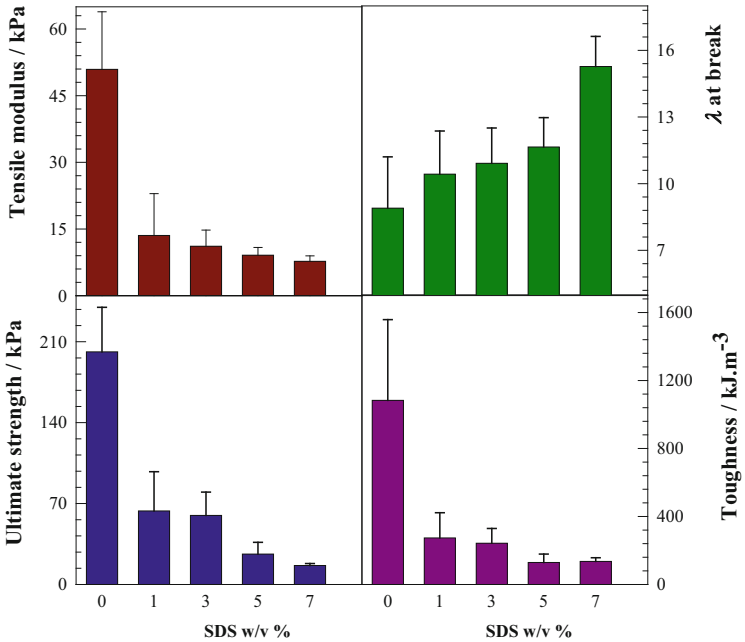

Fig. 18 Tensile modulus, elongation ratio λ at break, ultimate strength, and toughness of HM PAAm hydrogels prepared using 2 mol% of C17.3M plotted against their SDS contents; $C_0 = 10$ % (w/v). From [34] with permission from Elsevier

formed in CTAB–NaBr solutions. Dashed and solid curves show the data obtained from gels after preparation and in equilibrium with water, respectively. Extraction of free CTAB micelles from the physical gels results in a drastic increase in their Young's moduli (from 8–30 to 180–600 kPa) and tensile strengths (from 0.1–0.2 to 0.7–1.7 MPa) as a result of complex formation between PAAc and CTAB [42]. The largest modulus and fracture stress are 605 ± 20 kPa and 1.66 ± 0.24 MPa, respectively, obtained at the highest β ratio of 1/8.3. Such a drastic change in the mechanical properties of the gels upon immersion in water is a result of extraction of CTA counterions from the micelles by AAc anions and simultaneous formation of ionic bonds at neutral pH [42].

7.1 Large-Strain Properties

For a deeper understanding of the nature of physical cross-links in HM PAAm hydrogels, the gels were subjected to loading and unloading experiments [34]. Figure 20a, b shows the typical stress–strain curves of HM PAAm hydrogels from tensile tests composed of three repeated cycles [34]. The tests were conducted on

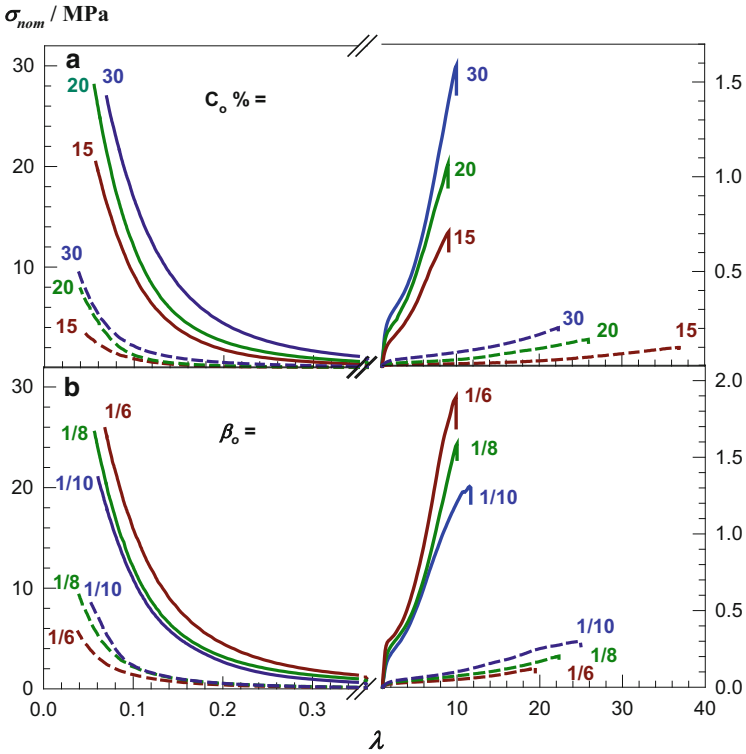

Fig. 19 Stress–strain curves of HM PAAc gels after preparation in CTAB solutions (*dashed curves*) and in equilibrium with water (*solid curves*) under compression ($\lambda < 1$) and elongation ($\lambda > 1$); C17.3M = 2 mol%, NaBr = 0.25 M. (**a**) $\beta_0 = 1/8$; percentage concentrations C_0 (w/v) as indicated. (**b**) $C_0 = 30$ % (w/v); β_0 values as indicated. From [42] with permission from the American Chemical Society

hydrogels with (Fig. 20a) and without surfactant (Fig. 20b) up to a stretch (λ_{max}) of 5, with a relaxation time of 7 min until the next tensile cycle started. The surfactant-containing hydrogel sample undergoes reversible cycles with a substantial hysteresis, revealing that the original microstructure can be restored by allowing the damaged hydrogel to rest for 7 min. Visually, it was observed that the residual stretch after each cycle decreases with increasing wait time between cycles and disappears after 7 min, so that the next loading curve follows the path of the first loading. In accord with DLS and rheological measurements, these cyclic tensile tests also indicate the existence of reversible cross-links in surfactant-containing hydrogels.

In contrast, the hydrogel sample without SDS behaves differently (Fig. 20b). Although the loading curve of the first tensile cycle is different from the unloading curve, and although a substantial hysteresis occurs (similar to that seen for the SDS-containing hydrogel), the subsequent cycles are nearly elastic with just a small amount of hysteresis; they also closely follow the path of the first unloading. This

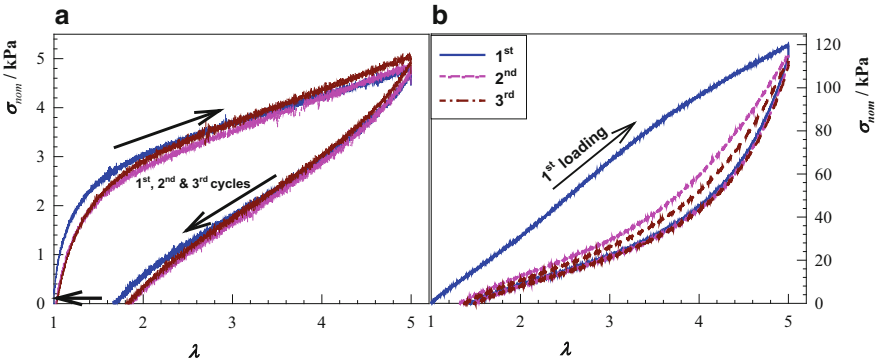

Fig. 20 (**a**, **b**) Loading–unloading curves of HM PAAm hydrogels with 7 % of SDS (**a**) and without SDS (**b**); $\lambda_{max} = 5$, C17.3M = 2 mol%. Waiting time between the cycles was 7 min. Cross-head speed was 50 mm min^{-1}. From [34] with permission from Elsevier

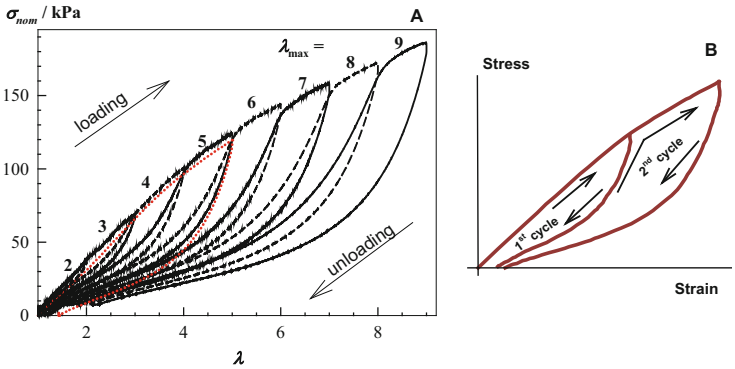

Fig. 21 (**a**) Eight successive loading–unloading cycles for different maximum strains (λ_{max}) as indicated on the curves. The *dotted red curve* represents the cycle conducted on a virgin gel sample ($\lambda_{max} = 5$). The tests were conducted using HM PAAm hydrogel samples without SDS; C17.3M = 2 mol%. (**b**) Idealized view of two successive cycles. From [34] with permission from Elsevier

finding indicates occurrence of an irrecoverable damage to the hydrogel sample during the first cycle, leading to a permanent residual elongation. In Fig. 21a, eight successive loading–unloading cycles are shown where the maximum strain, λ_{max}, increases from 2 to 9, corresponding to increasing elongation from 100 % to 800 % [34]. Successive cycles in Fig. 21a are represented by solid and dashed curves. Figure 21b shows an idealized view of two successive cycles. Each loading curve after the first cycle consists of two regions [34]:

1. Elastic region that closely follows the path of the unloading curve of the previous cycle
2. Damage region continuing the loading curve of the previous cycle

The passage from the elastic to the damage region takes place at the λ_{max} of the previous cycle. For instance, the loading curve of cycle 5 with $\lambda_{max} = 5$ follows the unloading and loading curves of cycle 4 between $\lambda = 1$–4 and $\lambda = 4$–5, respectively. This means that, because of the irreversible damage during the previous cycle, additional damage only occurs at a higher maximum strain. The dotted red curve in Fig. 21a shows the cycle conducted on a virgin hydrogel sample up to $\lambda_{max} = 5$. Because there was no previous damage to the gel sample, the loading curve follows the second region of the loading curves of cycles with $\lambda_{max} \leq 5$. Thus, the hysteresis of the first cycle is related to irreversible fracture of a part of the hydrophobic associations, whose extent increases with increasing λ_{max} during the loading step. This behavior is similar to that of double-network (DN) hydrogels [3, 98], where the first-cycle hysteresis occurs as a result of the irreversible fracture of covalent bonds in the highly cross-linked primary network.

Similar to the results of cyclic tensile tests, cyclic compression measurements also confirm the presence of reversibly breakable cross-links in hydrogels containing surfactant micelles. Figure 22a shows successive loading–unloading compression ($\lambda < 1$) and tensile cycles ($\lambda > 1$) of HM PDMA hydrogels containing 7 % of SDS [41]. The tests were carried out with increasing λ_{max} and with a waiting time of 7 min between cycles. In all cases, the loading curve of the compressive or tensile cycle is different from the unloading curve, indicating damage in the gel samples and dissipation of energy during the cycle. The good superposition of the successive loading curves demonstrates that the damage done to the gel samples during the loading cycle is recoverable. However, after swelling in water, these HM PDMA gels exhibit irreversible cycles with less significant hysteresis.

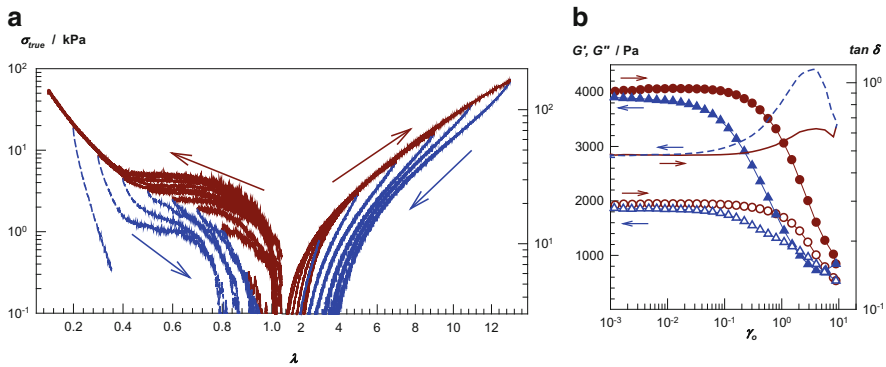

Fig. 22 (**a**) True stress (σ_{true}) versus deformation ratio (λ) of a surfactant-containing HM PDMA hydrogel from cyclic compression ($\lambda < 1$) and elongation ($\lambda > 1$) tests. The tests were conducted with increasing strain, with a waiting time of 7 min between cycles. (**b**) G' (*filled symbols*), G'' (*open symbols*), and tan δ (*curves*) of a HM PDMA hydrogel shown as a function of the strain (γ_0) at $\omega = 6.3$ rad s^{-1}. Sweep tests were conducted in up (*dark red circles*) and down directions (*blue triangles*), as indicated by the *arrows*; $C_0 = 15$ % (w/v), C17.3M = 2 mol%, SDS = 7 % (w/v), NaCl = 0.5 M. From [41] with permission from Elsevier

Strain-sweep tests conducted on HM PDMA hydrogels with 7 % (w/v) of SDS also demonstrate recoverability of the damage in the gel samples. Figure 22b shows up and down strain-sweep experiments, where the dynamic moduli G' and G'' together with the loss factor tan δ are plotted as a function of strain γ_0 [41]. The upward curves show a linear viscoelastic region at low strains ($\gamma_0 < 0.1$), beyond which the dynamic moduli decrease while the loss factor increases. Comparison of the up and down curves indicates that the gel exhibits an almost reversible strain-sweep spectrum; the breakdown of the microstructure caused by the strain is recovered at low strain amplitudes. Thus, this surfactant-containing HM PDMA hydrogel softens with increasing deformation and exhibits a liquid-like response (tan $\delta > 1$) at high strains, but reversibly; if the force is removed, the solution turns back to the same gel state.

The reversibility of the mechanical cycles of surfactant-containing gels indicates that the energy associated with the hysteresis is a result of the hydrophobic associations that break and reform dynamically, preventing fracture of the polymer backbone. The energy dissipated during the cycles, U_{hys}, is calculated from the area between the loading and unloading curves. Because uniaxial compression is equivalent to biaxial stretching [98], the maximum strain during compression (λ_{max}) is converted to the maximum biaxial extension ratio ($\lambda_{biax,max}$) by $\lambda_{biax,max} = \lambda_{max}^{-0.5}$. In Fig. 23a, the hysteresis energies (U_{hys}) calculated from the cycles in Fig. 22a are plotted against the maximum strain in terms of uniaxial (λ_{max}) and biaxial ($\lambda_{biax,max}$) extension ratios. All U_{hys} data collapse onto a single curve; hence, the hysteresis energy only depends on the maximum extension of the polymer chains.

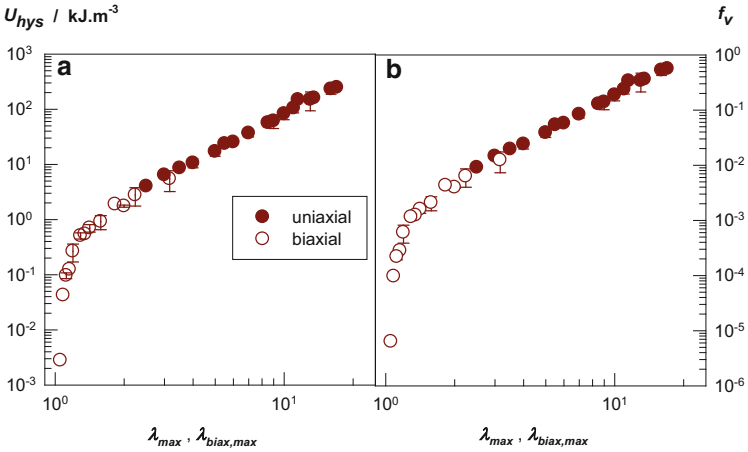

Fig. 23 (**a**) Hysteresis energy U_{hys} and (**b**) fraction f_v of dissociated cross-links during loading–unloading compression (*open symbols*) and elongation cycles (*filled symbols*) of a surfactant-containing HM PDMA hydrogel, shown as a function of the maximum strain λ_{max} or $\lambda_{biax,\ max}$; $C_0 = 15$ % (w/v), C17.3M = 2 mol%, SDS = 7 % (w/v), NaCl = 0.5 M. From [41] with permission from Elsevier

The energy dissipated during the reversible cycles (U_{hys}) can be interpreted as the sum of the dissociation energies of hydrophobic associations broken down reversibly during the cyclic tests [98, 99]:

$$U_{hys} = U_{xl} \nu_e f_\nu \tag{5a}$$

where U_{xl} is the average dissociation energy of a single association (~10^2 kJ mol^{-1} [44, 100]), ν_e is the cross-linking density of the gel (i.e., the concentration of elastically effective hydrophobic associations), and f_ν is the fraction of associations broken during the loading. The cross-linking density of the hydrogels, ν_e, can be estimated from their shear moduli, G [101, 102]:

$$G = \nu_e RT \tag{5b}$$

where R and T represent their usual meanings. Equation (5b) assumes affine deformation of the network chains, which is a reasonable assumption for physical gels formed by hydrophobic associations [33]. Using the values of U_{hys} and ν_e together with Eq. (5a), one can estimate the fraction of physical cross-links reversibly broken during the mechanical cycles (f_ν). In Fig. 23b, f_ν is plotted against the maximum strain (λ_{max} or $\lambda_{biax,max}$) achieved during the tensile and compression cycles in Fig. 22a [41]. Like the hysteresis energy (Fig. 23a), f_ν only depends on the maximum strain, indicating that the maximum extension ratio of the chains is the only parameter controlling the fraction of physical cross-links broken during loading. Thus, both compression and elongation have the same effect on the physical cross-links of hydrogels formed by hydrophobic associations. Figure 23b also shows that f_ν varies between 10^{-6} and 10^0, indicating that all of the physical cross-links can dissociate under force, but they reversibly reform if the force is removed.

The cyclic mechanical test results presented above demonstrate the existence of reversibly breakable cross-links in surfactant-containing hydrogels. In such hydrogels, a large portion of the physical cross-links dissociate under force, but they do so reversibly: if the force is removed, they reform again. However, swelling in water (i.e., extraction of surfactant micelles from the physical network) results in loss of the reversible nature of the cross-linking as a result of an increase in the lifetime of the hydrophobic associations. Thus, one may propose that when the surfactant alkyl chains are trapped electrostatically in an ionic hydrogel formed via hydrophobic interactions, the cross-links in the resulting gel system exhibit reversible behavior both after preparation and after swelling in water. This was indeed observed [42]. HM PAAc hydrogels formed in CTAB solutions exhibit reversible cycles, both at the state of preparation and in equilibrium in water. The hysteresis energy (U_{hys}) of these gels in equilibrium with water is about one order of magnitude larger than that of the gels after preparation, indicating formation of a larger number of reversibly breakable cross-links upon gel swelling [42].

8 Self-Healing

The reversible manner of disengagement of the hydrophobic units of surfactant-containing physical gels under an external force forms a basis for their self-healing. Figure 24 shows photographs of typical healing processes of HM PAAm hydrogels [32, 33]. First, hydrogel samples were cut into two separate parts using a blade. Then the two parts were put into contact and allowed to stand at 24 °C. After a few minutes, it was not possible to separate the two parts by stretching manually. However, in accord with the cyclic test results, such autonomous self-healing did not occur in surfactant-free hydrogels [33].

The self-healing efficiency of HM PAAm hydrogels was quantified by uniaxial tensile tests conducted on virgin and healed gel samples [33]. The healing efficiency of surfactant-containing hydrogels depends on several factors, including the healing time, the polymer and surfactant contents of the hydrogels, and the type and amount of the hydrophobes. Figure 25 shows the elongation at break of healed hydrogels, denoted by λ_b, as a function of the healing time [33]. The value of λ_b rapidly increases with the healing time and, after 20 min, it approaches that of the virgin gel sample $\lambda_{b,0}$, as represented by the horizontal solid line in Fig. 25. As the inset to Fig. 25 demonstrates, the healing efficiency markedly decreases with increasing polymer concentration of the gels. The efficiency also crucially depends on the comonomer feed composition; efficiency decreases as the amount of hydrophobe in the feed increases (i.e., as the fraction of dissociable cross-links decreases) [33].

As mentioned in the previous section, surfactant-containing HM PDMA hydrogels exhibit a high stretchability 4,200 ± 400 % as a result of additional hydrogen bonding and hydrophobic interactions between the DMA units. It was shown that this high stretchability can be recovered autonomously after sample damage after just a short healing time. In Fig. 26a, stress–strain curves of virgin and healed HM PDMA hydrogel samples are shown for different healing times [41]. In Fig. 26b, the tensile modulus (E), the fracture stress (σ_f), and the elongation ratio at

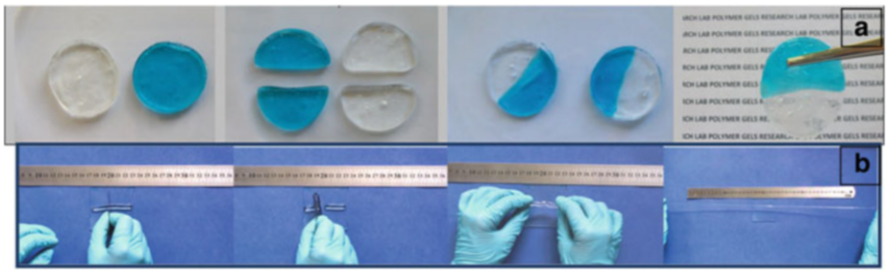

Fig. 24 (**a**, **b**) Autonomous self-healing of HM PAAm hydrogels formed using 2 mol% of C17.3M hydrophobe in 7 % SDS + 0.5 M NaCl solution; $C_0 = 5$ % (**a**) and 10 % (**b**). In (**a**), one of the hydrogel samples is colored for clarity. From [32, 33] with permission from the American Chemical Society

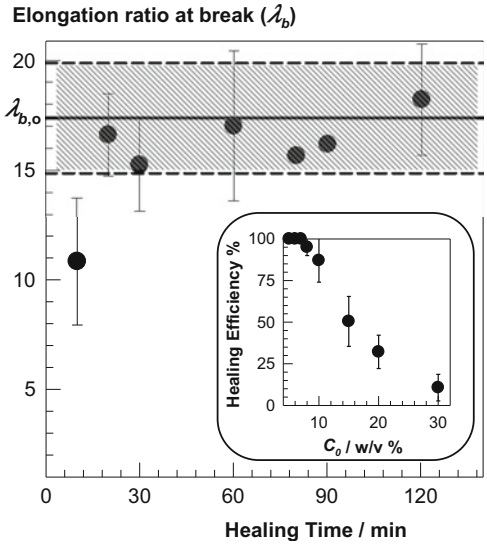

Fig. 25 Elongation at break of healed HM PAAm gels (λ_b) plotted against the healing time; $C_0 = 10$ %, C17.3M = 2 mol%, SDS = 7 %, NaCl = 0.5 M. The *horizontal line* represents λ_b of the virgin sample, denoted by $\lambda_{b,0}$. The *dashed area* represents its standard deviation. The *inset* illustrates the healing efficiency of the hydrogels as a function of C_0; healing time = 30 min. From [33] with permission from the American Chemical Society

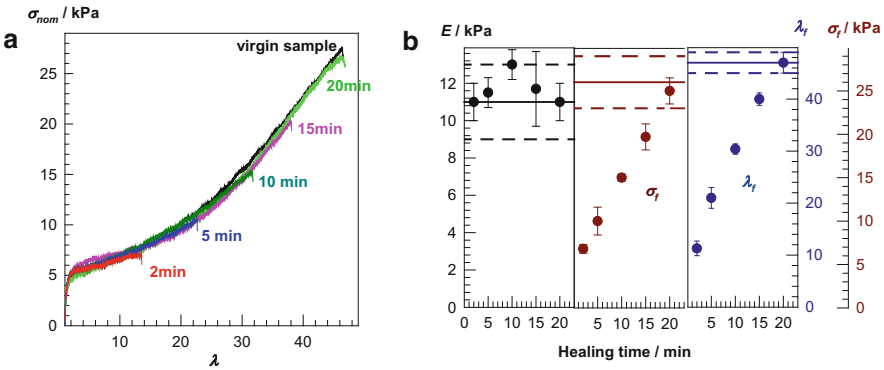

Fig. 26 (**a**) Stress–strain curves of virgin and healed HM PDMA hydrogel samples after preparation; $C_0 = 15$ % (w/v), C17.3M = 2 mol%, SDS = 7 % (w/v), NaCl = 0.5 M. Healing times are indicated next to the curves; temperature = 24 °C. (**b**) Tensile modulus E, tensile fracture stress σ_f, and elongation ratio λ_f at break of healed HM PDMA gels plotted against the healing time. The behavior of the original gel sample is represented by the *solid lines*. The *dashed lines* indicate the corresponding standard deviations. From [41] with permission from Elsevier

break (λ_f), of the healed gel samples are plotted as a function of the healing time. The modulus E is recovered within 2 min, indicating a very rapid and autonomous self-healing process in the PDMA hydrogel. After 10 min, the fracture stress of the

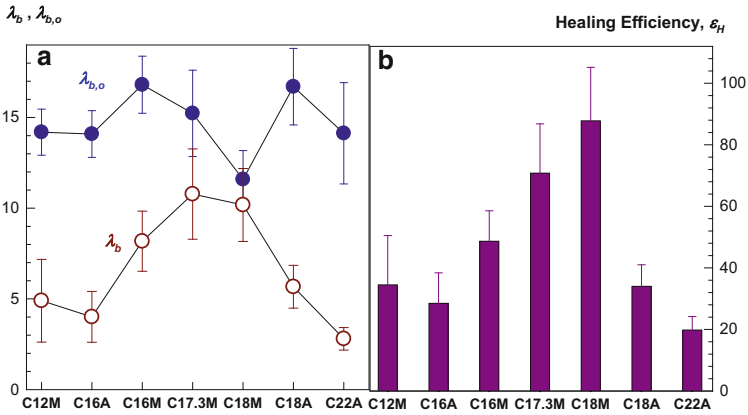

Fig. 27 (**a**) Elongation at break of healed (λ_b) and original ($\lambda_{b,0}$) HM PAAm gel samples. (**b**) Healing efficiency ε_H for gels prepared using seven different hydrophobes in 7 % SDS + 0.5 M NaCl solution; hydrophobe content = 2 mol%. From [34] with permission from Elsevier

healed gel is 15 kPa, which is 60 % of the fracture stress of the virgin sample. A healing time of 20 min suffices to recover all the initial mechanical properties of the physical hydrogel.

The side chain length of the hydrophobic monomers is another structural parameter that is crucially important for obtaining self-healing hydrogels with a high autonomic healing efficiency [34]. Figure 27a shows the elongation at break of HM PAAm hydrogel samples prepared using 2 mol% hydrophobic monomer of various alkyl side chain length. The data denoted by λ_b and $\lambda_{b,0}$ in Fig. 27a are obtained from the healed and virgin gels, respectively. The healing efficiencies of the hydrogels (ε_H), calculated as $\varepsilon_H = (\lambda_b/\lambda_{b,0}) \times 10^2$, are shown in Fig. 27b. The value of λ_b approaches $\lambda_{b,0}$, that is, ε_H increases as the length of the alkyl side chain increases. A maximum healing efficiency is found in the physical hydrogel prepared with C18M hydrophobe [34]. At longer side chain lengths, the healing efficiency decreases again. This indicates that the self-healing ability of the hydrogels depends critically on the length of alkyl side chains. Hydrophobes with an alkyl side chain of 18 carbons produce the strongest self-healing in these physical hydrogels.

Figure 27 also shows that hydrophobic monomers with methacrylate groups produce physical hydrogels with a higher healing efficiency than those with acrylate groups. For example, at an alkyl side chain length of 18 carbons, the efficiency of healing rises from 34 % to 88 % if acrylate (C18A) is replaced by methacrylate (C18M). A similar tendency is seen for hydrogels prepared with either C16A or C16M hydrophobic monomers (29 % versus 49 %). The restricted mobility of the methacrylate backbones as compared to acrylates is probably responsible for this behavior. Previous studies on side-chain crystalline polymers indeed show that hydrophobic methacrylates produce polymers with a lesser degree of crystallinity than the corresponding acrylates [103]. This indicates that the methacrylate

backbone restricts molecular mobility and the ability of alkyl side chains to align. Thus, the number of hydrophobic associations decreases while the fraction of free hydrophobic blocks increases in hydrogels formed by hydrophobic methacrylates. Lower tensile strength and a higher tan δ of gels prepared using hydrophobes with methacrylate groups indicate a larger number of free associative groups and also confirm this picture (Fig. 16a). Thus, as the number of free hydrophobic blocks at the cut surfaces increases, they find their partners much faster so that hydrogels prepared by methacrylates exhibit higher self-healing efficiencies than acrylate-based gels that have lower numbers of nonassociated blocks.

The autonomous self-healing efficiency of hydrophobically modified hydrogels decreases as their mechanical strength is increased. This is a result of the antagonistic feature of the self-healing ability to the mechanical strength of these hydrogels. For instance, the efficiency of self-healing increases with decreasing lifetime of dynamic cross-links in the gel because of favorable chain diffusion across fractured gel surfaces [34]. However, hydrogels with short-living cross-links necessarily become mechanically weak on experimental time scales. It was shown that self-healing in mechanically strong hydrogels can be induced by an external stimulus such as temperature or addition of a healing agent. Figure 28a illustrates stress–strain data of virgin HM PAAc gel samples (solid curves) together with those of healed samples at various temperatures (dashed curves) [39]. In Fig. 28b, the efficiency of healing based on the recovered fracture stress is plotted as a function of the healing temperature. Without any external stimulus, healed gels formed at $C_0 = 15$ % (w/v) withstand 10 kPa stress, that is, autonomous self-healing takes place with an efficiency of 60 %. Increasing C_0 from 15 % to 30 % also increases the fracture stress of self-healed gels up to 40 kPa while the healing efficiency

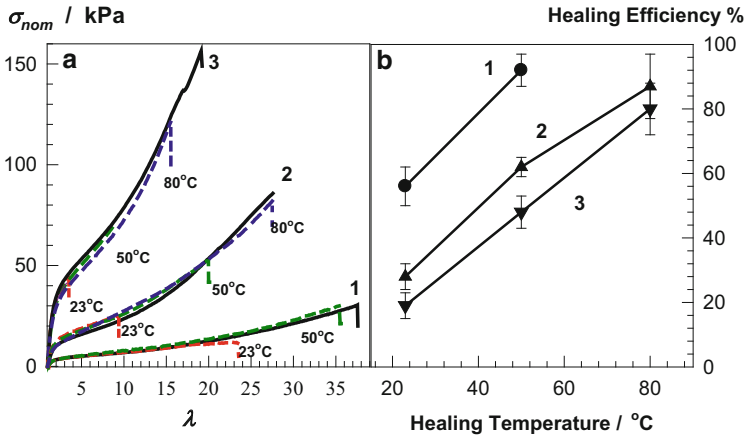

Fig. 28 (**a**) Stress–strain curves of virgin (*solid curves*) and healed surfactant-containing HM PAAc gel samples (*dashed curves*). Healing temperatures are indicated next to the curves; C17.3M = 2 mol%. (**b**) Efficiency of healing of hydrogel samples plotted against the healing temperature; healing time = 30 min. (**a**, **b**) $C_0 = 15$ % (*1*), 20 % (*2*), and 30 % (w/v) (*3*). From [39] with permission from the Royal Society of Chemistry

decreases to 20 %. This is a result of the simultaneous increase in the cross-linking density of the hydrogels, reducing the chain mobility [39]. Figure 28 also shows that the efficiency of healing increases remarkably as the temperature is increased. For instance, at $C_0 = 30$ % (w/v), gels healed at 23 °C fail upon application of 42 ± 5 kPa stress, whereas those healed at 80 °C withstand more than 120 kPa of stress. All the hydrogel samples self-heal with at least 80 % efficiency at 80 °C. The primary mechanism of temperature-induced healing in HM PAAc hydrogels is attributed to increased solubility of hydrophobic moieties in aqueous solutions, leading to a decrease in the association degree of the polymers [52]. Thus, increasing ability of the hydrogels to self-heal at a high temperature is a result of a decrease in the lifetime of hydrophobic associations, as already observed in semidilute solutions of HM PAAms [52, 104]. This simultaneously increases the chain mobility, so that the polymer chains on the two cut surfaces can easily diffuse from one side to the other, and the hydrophobes across the ruptured interface become more accessible to each other. Indeed, the dynamic moduli of HM PAAc gels sharply decrease with increasing temperature, indicating that the gels become weak with rising temperature [39, 42].

Another stimulus to trigger self-healing in hydrogels formed via hydrophobic interactions is the treatment of the damaged area of the gels with an aqueous solution of wormlike surfactant micelles [40]. In Fig. 29a, stress–strain curves of a virgin HM PAAm gel sample without SDS (dashed curve) and gel samples healed by addition of an SDS solution (solid curves) are shown. The fracture stress after 1 h of healing is 25 ± 5 kPa, which is almost twice the fracture stress of the virgin gel sample containing SDS [40]. For healing times ranging from 30 min to 9 h, the healed region of the gels is more swollen than the gel bulk region. This is due to

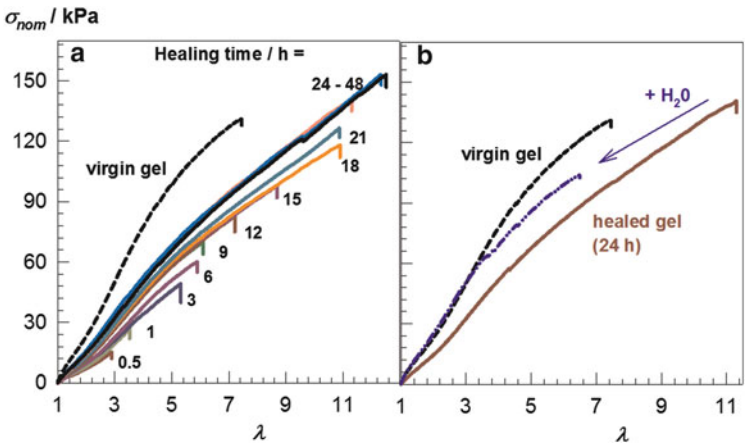

Fig. 29 (**a**, **b**) Stress–strain curves of a virgin HM PAAm gel sample without SDS (*dashed curve*) and healed gel samples (*solid curves*). Healing times are indicated next to the curves. The *blue* (*dash-dot*) *curve* in (**b**) represents the stress–strain data of a gel sample healed for 24 h and then immersed in an excess of water for 2 weeks to extract SDS prior to the mechanical tests. From [40] with permission from Springer

absorption of SDS by the polymer at the welded interface, producing an excess of counterion concentration inside the gel and leading to increased gel swelling [40]. This interface also acts as a weak point in the healed gels, so that they always rupture at this region. However, for longer healing times (>9 h), the welded interface deswells again and becomes identical to the bulk region. Simultaneously, the healed gel samples rupture in the bulk region, while the welded interface remains unbroken. For all healing times indicated in Fig. 29a, the surfactant-mediated healing is irreversible: when immersed in water to extract the healing agent, the healed gel samples remain as stable as the virgin gels [40].

Figure 29a also shows that both the fracture stress and the elongation at break of the gel samples rapidly increase with increasing healing time, and after 20 h they reach the values of the virgin gel sample. For longer healing times, the gel samples become stronger and tougher than the original gel, while the moduli of the healed gels partially recover their original values. This was attributed to the presence of SDS in the healed gel samples, weakening their hydrophobic interactions [40]. Indeed, when the healed samples are immersed in an excess of water to extract SDS micelles, their stress–strain curves approach the curve of the virgin sample. This is illustrated by the blue (dash-dot) curve in Fig. 29b, representing the stress–strain data of a gel sample healed for 24 h and then immersed in an excess of water for 2 weeks to extract SDS prior to the mechanical tests. Both the fracture stress and the elongation at break are 80 % of the original values. In conclusion, because the surfactant-induced healing technique is applicable to physical gels formed by hydrophobic associations, it overcomes the requirement of the presence of surfactants in the gels for their healing, thereby allowing applications in aqueous environment.

High-strength PAAc hydrogels formed in oppositely charged surfactant solutions can also be healed by treatment of cut surfaces with surfactant solutions [42]. In Fig. 30, the stress–strain curves of virgin and healed PAAc gel samples

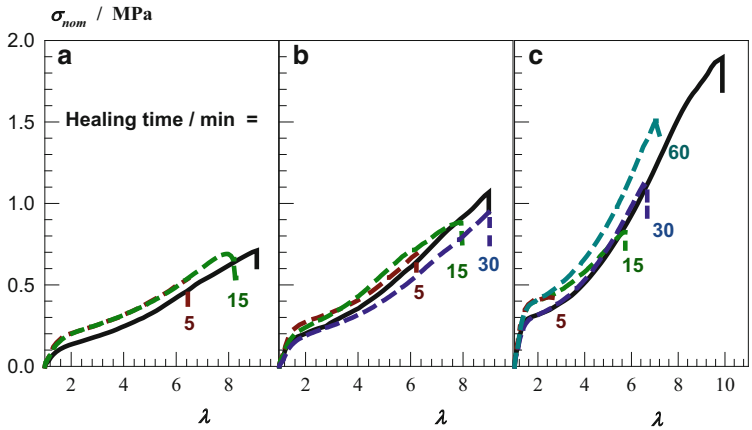

Fig. 30 (**a–c**) Stress–strain curves of virgin (*solid curves*) and healed HM PAAc gel samples in equilibrium with water (*dashed curves*): (**a**) $C_0 = 15$ %, $\beta_0 = 1/8$; (**b**) $C_0 = 20$ %, $\beta_0 = 1/8$; (**c**) $C_0 = 30$ %, $\beta_0 = 1/6$. From [42] with permission from the American Chemical Society

in equilibrium with water are shown for various healing times in surfactant solutions. The fracture stress of the healed gels increases with increasing healing time or with increasing PAAc concentration. After a healing time of 60 min, the hydrogel sample formed at $C_0 = 30$ % and $\beta_0 = 1/6$ sustains 1.5 ± 0.2 MPa stresses and ruptures at a stretch of 7 ± 1 (Fig. 30c) [42]. To our knowledge, this fracture stress is the highest value reported in the literature.

The hydrophobe content of the self-healing hydrogels described above is 2 mol % (relative to the amount of monomers in total). It was shown that at a high hydrophobe level, hydrogels containing crystalline domains and exhibiting shape memory properties can be obtained [38]. These hydrogels can also be healed by treatment of a potentially damaged area with surfactant solutions. Such self-healing hydrogels with shape memory behavior were prepared by copolymerization of AAc with 20–50 mol% of C18A in aqueous SDS–NaCl solutions [38]. After extraction of the surfactant micelles, these HM PAAc hydrogels possess 60–70 % of water and exhibit three orders of magnitude change in their elastic moduli when the temperature changes between below and above the melting temperature of the crystalline domains (~50 °C). In addition, these hydrogels exhibit complete shape recovery to the permanent shape at 60 °C, together with surfactant-triggered self-healing. The blocky structure of the HM PAAc chains formed by micellar polymerization is responsible for the drastic change in their mechanical properties and for their significant shape memory effect.

9 Concluding Remarks

In this chapter, recent developments in the design of hydrogels formed via hydrophobic interactions are reviewed, with a special emphasis on the function of surfactant in their dynamic and mechanical properties. Micellar copolymerization is a simple technique for the synthesis of such hydrogels. A particular advantage of this technique is the blocky structure of the resulting hydrophobically modified polymers, significantly enhancing their associative properties.

Because preparation of mechanically strong hydrogels via micellar copolymerization requires blocks of large hydrophobes, salts such as NaCl or NaBr should be included in the micellar solution. These salts screen electrostatic interactions, causing the micelles to grow. In turn, the growth of the micelles provides solubilization of substantial amounts of hydrophobic monomers in the aqueous solution. After solubilization of large hydrophobes within wormlike surfactant micelles of salt solutions, they can be copolymerized with hydrophilic monomers to obtain hydrophobically modified hydrogels with tunable properties.

Hydrogels formed via hydrophobic interactions in aqueous micellar solutions present two faces, depending on which state they are in. These states are (i) the preparation state, when the gels contain surfactant micelles, and (ii) the state in equilibrium with pure water, when the free surfactant micelles have been removed after preparation.

At the state of preparation, the hydrogels exhibit a slow mode in DLS, independent of the scattering vector, that is related to structural relaxation of their physical polymer network. This relaxation only occurs in the presence of surfactant micelles and disappears when SDS is removed. A gel containing surfactant micelles exhibits time-dependent dynamic moduli with a plateau modulus at high frequencies and a loss factor above 0.1. After removal of the surfactants, the dynamic moduli become nearly independent of time, and the loss factor decreases to below 0.1, corresponding to solid-like behavior. Simultaneously, the degree of spatial gel inhomogeneity increases considerably after extraction of surfactant molecules, also demonstrating a loss of reversibility of the cross-linkages.

Thus, with surfactants, the cross-links are reversible as a result of local solubilization of the hydrophobic associations, so that the hydrogels are weak. After removal of surfactant, however, direct exposure of the hydrophobic associations to the aqueous environment increases their lifetimes so that the hydrogels behave mostly like chemical gels with time-independent dynamic moduli and a single relaxation mode in DLS. These findings also demonstrate that the presence of surfactant micelles is responsible for the slow mode of the physical hydrogels. Because breakup of a micelle around the hydrophobic blocks enhances the hydrophobic interactions at this location, while its re-formation re-decreases these interactions, the micellar kinetics and resulting temporary strong associations are responsible for the slow network relaxation in surfactant-containing physical gels.

Hydrophobically modified ionic hydrogels formed in oppositely charged surfactant solutions exhibit frequency-dependent dynamic moduli if they are in equilibrium in water after extraction of free surfactant micelles. This is a result of complex formation between the ionic polymer and the oppositely charged surfactant, leading to polymer-bound surfactant counterions in the hydrogels.

The mechanical strength of hydrogels formed using hydrophobic acrylates is higher than that of those formed using methacrylates. This is due to the limited flexibility of the methacrylate backbones, reducing the number of hydrophobic associations acting as physical cross-links. Similarly, the length of the alkyl side chain of the hydrophobes as well as the type of hydrophilic chains also affect the mechanical performance of hydrogels formed via hydrophobic interactions. For instance, replacing PAAm by PAAc leads to mechanically stronger hydrogels because of stabilization of the cross-linking hydrophobic associations by cooperative hydrogen bonding between carboxyl groups. A similar improvement of the mechanical performance is observed by replacement of PAAm by PDMA as a result of additional hydrophobic interactions between the DMA units. Moreover, because the dynamic features of the hydrogels drastically change after removal of surfactant micelles, similar changes are also observed in their mechanical properties. Most importantly, a remarkable decrease in the stretchability of such hydrogels is observed upon extraction of surfactant micelles. Ionic hydrogels formed in oppositely charged surfactant solutions exhibit a significant enhancement in their mechanical properties when they are immersed in water. This is a result of extraction of surfactant counterions from the micelles and simultaneous formation of ionic bonds. By tuning the preparation conditions, hydrogels formed via

hydrophobic interactions in micellar solutions exhibit a high stretchability (up to 5,000 %), high mechanical strength (up to 1.7 MPa tensile stress), and complete autonomous self-healing ability.

Current research in the field of self-healing hydrogels is focused on improving the mechanical performance of self-healing gels formed via reversible molecular interactions. Because self-healing of a hydrogel is opposite to its mechanical strength, the magnitude of the tensile strength recovered after repair for most healable hydrogels is below 0.4 MPa. As discussed in this chapter, hydrophobically modified hydrogels that are self-healed via heating and surfactant treatment of the damaged areas withstand up to 1.5 MPa stresses and rupture at a stretch of 600 %. Thus, hydrogels formed via hydrophobic interactions combine good mechanical properties with a high self-healing efficiency and are promising materials for new technologies.

Acknowledgement Work was supported by the Scientific and Technical Research Council of Turkey (TUBITAK, KBAG–114Z312). The author thanks the Turkish Academy of Sciences (TUBA) for partial support.

References

1. Okay O (2009) General properties of hydrogels. In: Gerlach G, Arndt K-F (eds) Hydrogel sensors and actuators, Springer series on chemical sensors and biosensors, vol 6. Springer, Berlin, pp 1–14
2. Ahagon A, Gent AN (1975) J Polym Sci Polym Phys Ed 13:1903
3. Brown HR (2007) Macromolecules 40:3815
4. Abdurrahmanoglu S, Can V, Okay O (2009) Polymer 50:5449
5. Gong JP, Katsuyama Y, Kurokawa T, Osada Y (2003) Adv Mater 15:1155
6. Tanaka Y, Gong JP, Osada Y (2005) Prog Polym Sci 30:1
7. Okumura Y, Ito K (2001) Adv Mater 13:485
8. Miquelard-Garnier G, Demoures S, Creton C, Hourdet D (2006) Macromolecules 39:8128
9. Haraguchi K, Takehisa T (2002) Adv Mater 14:1120
10. Huang T, Xu H, Jiao K, Zhu L, Brown HR, Wang H (2007) Adv Mater 19:1622
11. Deng G, Tang C, Li F, Jiang H, Chen Y (2010) Macromolecules 43:1191
12. Phadke A, Zhang C, Arman B, Hsu C-C, Mashelkar A, Lele AK, Tauber MJ, Arya G, Varghese S (2012) Proc Natl Acad Sci USA 109:4383
13. Zhang H, Xia H, Zhao Y (2012) ACS Macro Lett 1:1233
14. Cui J, del Campo A (2012) Chem Commun 48:9302
15. Liu J, Song G, He C, Wang H (2013) Macromol Rapid Commun 34:1002
16. Haraguchi K, Uyama K, Tanimoto H (2011) Macromol Rapid Commun 32:1253
17. South AB, Lyon LA (2010) Angew Chem Int Ed 49:767
18. Wang Q, Mynar JL, Yoshida M, Lee E, Lee M, Okura K, Kinbara K, Aida T (2010) Nature 463:339
19. Sun J-Y, Zhao X, Illeperuma WRK, Chaudhuri O, Oh KH, Money DJ, Vlassak JJ, Suo Z (2012) Nature 489:133
20. Foo CTSWP, Lee JS, Mulyasasmita W, Parisi-Amon A, Heilshorn SC (2009) Proc Natl Acad Sci USA 106:22067
21. Appel EA, Biedermann F, Rauwald U, Jones ST, Zayed JM, Scherman OA (2010) J Am Chem Soc 132:14251

22. Skrzeszewska PJ, Sprakel J, Wolf FA, Fokkink R, Stuart MAC, van de Gucht J (2010) Macromolecules 43:3542
23. Holten-Andersen N, Harrington MJ, Birkedal H, Lee BP, Messersmith PB, Lee KYC, Waite JH (2011) Proc Natl Acad Sci USA 108:2651
24. Shafiq Z, Cui J, Pastor-Perez L, San Miguel V, Gropeanu RA, Serrano C, del Campo A (2012) Angew Chem Int Ed 124:4408
25. Xu Y, Wu Q, Sun Y, Bai H, Shi G (2010) ACS Nano 4:7358
26. Liu F, Li F, Deng G, Chen Y, Zhang B, Zhang J, Liu C-Y (2012) Macromolecules 45:1636
27. Zhang Y, Tao L, Li S, Wei Y (2011) Biomacromolecules 12:2894
28. He L, Fullenkamp DE, Rivera JG, Messersmith PB (2011) Chem Commun 47:7497
29. Froimowicz P, Klinger D, Landfester K (2011) Chem Eur J 17:12465
30. Quint SB, Pacholski C (2011) Soft Matter 7:3735
31. Abdurrahmanoglu S, Cilingir M, Okay O (2011) Polymer 52:694
32. Tuncaboylu DC, Sari M, Oppermann W, Okay O (2011) Macromolecules 44:4997
33. Tuncaboylu DC, Sahin M, Argun A, Oppermann W, Okay O (2012) Macromolecules 45: 1991
34. Tuncaboylu DC, Argun A, Sahin M, Sari M, Okay O (2012) Polymer 53:5513
35. Tuncaboylu DC, Argun A, Algi MP, Okay O (2013) Polymer 54:6381
36. Baskan T, Tuncaboylu DC, Okay O (2013) Polymer 54:2979
37. Akay G, Hassan-Raeisi A, Tuncaboylu DC, Orakdogen N, Abdurrahmanoglu S, Oppermann W, Okay O (2013) Soft Matter 9:2254
38. Bilici C, Okay O (2013) Macromolecules 46:3125
39. Gulyuz U, Okay O (2013) Soft Matter 9:10287
40. Argun A, Algi MP, Tuncaboylu DC, Okay O (2014) Colloid Polym Sci 292:511
41. Algi MP, Okay O (2014) Eur Polym J 59:113
42. Gulyuz U, Okay O (2014) Macromolecules 47:6889
43. Tanaka F, Edwards SF (1992) Macromolecules 25:1516
44. Annable T, Buscall R, Ettelaie R, Whittlestone D (1993) J Rheol 37:695
45. Bell GI (1978) Science 178:618
46. Pham QT, Russel WB, Thibeault JC, Lau W (1999) Macromolecules 32:5139
47. Tripathi A, Tam KC, McKinley GH (2006) Macromolecules 39:1981
48. Tian J, Seery TAP, Weiss RA (2004) Macromolecules 37:10001
49. Hao J, Weiss RA (2011) Macromolecules 44:9390
50. Matsuda A, Sato J, Yasunaga H, Osada Y (1994) Macromolecules 27:7695
51. Hill A, Candau F, Selb J (1993) Macromolecules 26:4521
52. Volpert E, Selb J, Candau F (1998) Polymer 39:1025
53. Regalado EJ, Selb J, Candau F (1999) Macromolecules 32:8580
54. Candau F, Selb J (1999) Adv Colloid Interface Sci 79:149
55. Gao B, Guo H, Wang J, Zhang Y (2008) Macromolecules 41:2890
56. Candau F, Regalado EJ, Selb J (1998) Macromolecules 31:5550
57. Kujawa P, Audibert-Hayet A, Selb J, Candau F (2004) J Polym Sci B Polym Phys 42:1640
58. Kujawa P, Audibert-Hayet A, Selb J, Candau F (2006) Macromolecules 39:384
59. Beyer K, Leine D, Blume A (2006) Colloids Surf B Biointerfaces 49:31
60. Chern CS, Chen TJ (1998) Colloids Surf A Physicochem Eng Aspects 138:65
61. Leyrer RJ, Machtle W (2000) Macromol Chem Phys 201:1235
62. Lau W (2002) Macromol Symp 182:283
63. Rehage H, Hoffman H (1991) Mol Phys 74:933
64. Magid LJ (1998) J Phys Chem B 102:4064
65. Hassan PA, Raghauan SR, Kaler EW (2002) Langmuir 18:2543
66. Missel PJ, Mazer NA, Benedek GB, Young CY (1980) J Phys Chem 84:1044
67. Sutherland E, Mercer SM, Everist M, Leaist D (2009) J Chem Eng Data 54:272
68. Mazer NA, Benedek GB, Carey MC (1976) J Phys Chem 80:1075
69. Young CY, Missel PJ, Mazer NA, Benedek GB, Carey MC (1978) J Phys Chem 82:1375

70. Pecora R (1985) Dynamic light scattering: application of photon correlation spectroscopy. Plenum, New York
71. Molchanov VS, Philippova OE, Khokhlov AR, Kovalev YA, Kuklin AI (2007) Langmuir 23:105
72. Kumar S, Bansal D, Din K (1999) Langmuir 15:4960
73. Kunieda H, Ozawa K, Huang K-L (1998) J Phys Chem B 102:831
74. Siriwatwechakul W, LaFleur T, Prud'homme RK, Sullivan P (2004) Langmuir 20:8970
75. Sato T, Acharya DP, Kaneko M, Aramaki K, Singh Y, Ishitobi M, Kunieda HJ (2006) J Dispers Sci Technol 27:611
76. Törnblom M, Henriksson U, Ginley M (1994) J Phys Chem 98:7041
77. Wang F, Chen T, Shang Y, Liu H (2011) Korean J Chem Eng 28:923
78. Zhang S, Teng HN (2008) Colloid J 70:105
79. Tah B, Pal P, Mahato M, Talapatra GB (2011) J Phys Chem B 115:8493
80. Marrucci G, Bhargava S, Cooper SL (1993) Macromolecules 26:6483
81. Patruyo LG, Muller AJ, Saez AE (2002) Polymer 43:6481
82. Penott-Chang EK, Gouveia L, Fernandez IJ, Muller AJ, Diaz-Barrios AD, Saez AE (2007) Colloids Surf A Physicochem Eng Aspects 295:99
83. Magny B, Iliopoulos I, Zana R, Audebert R (1994) Langmuir 10:3180
84. Philippova OE, Hourdet D, Audebert R, Khokhlov AR (1996) Macromolecules 29:2822
85. Hayashi S, Ikeda S (1980) J Phys Chem 84:744
86. Patist A, Oh SG, Leung R, Shah DO (2001) Colloids Surf A Physicochem Eng Aspects 176:3
87. Williams G, Watts DC (1970) Trans Faraday Soc 66:80
88. Gurtovenko AA, Gotlib YY (2001) J Chem Phys 115:6785
89. Ng TSK, McKinley GH (2008) J Rheol 52:417
90. Bastide J, Candau SJ (1996) Structure of gels as investigated by means of static scattering techniques. In: Cohen Addad JP (ed) Physical properties of polymeric gels. Wiley, New York, p 143
91. Shibayama M (1998) Macromol Chem Phys 199:1
92. Shibayama M, Ikkai F, Nomura S (1994) Macromolecules 27:6383
93. Lindemann B, Schröder UP, Oppermann W (1997) Macromolecules 30:4073
94. Kizilay MY, Okay O (2003) Macromolecules 36:6856
95. Joosten JGH, Mccarthy JL, Pusey PN (1991) Macromolecules 24:6690
96. Pusey PN, van Megen W (1989) Phys A 157:705
97. Ikkai F, Shibayama M (1999) Phys Rev Lett 82:4946
98. Webber RE, Creton C, Brown HR, Gong JP (2007) Macromolecules 40:2919
99. Lake GJ, Thomas AG (1967) Proc R Soc Lond A 300:108
100. Ng WK, Tam KC, Jenkins RD (2000) J Rheol 44:137
101. Flory PJ (1953) Principles of polymer chemistry. Cornell University Press, Ithaca, NY
102. Treloar LRG (1975) The physics of rubber elasticity. University Press, Oxford
103. Livshin S, Silverstein MS (2007) Macromolecules 40:6349
104. Biggs S, Selb J, Candau F (1993) Polymer 34:580